RSC Applied Polymers

ROYAL SOCIETY OF CHEMISTRY

PAPER

View Article Online
View Journal

Cite this: DOI: 10.1039/d6lp00109b

Degradable polyester ternary blends: composition and hybrid compatibilization for flexible packaging

Matias Menossi, †[a,b] Manushri Gunasekaran,†[a,b] Ehsan Pesaranhajiabbas,[a,b] Amar K. Mohanty *[a,b] and Manjusri Misra *[a,b]

A fully degradable ternary blend system comprising bio-based poly(butylene succinate) (BioPBS), poly (butylene adipate-*co*-terephthalate) (PBAT), and poly(3-hydroxybutyrate-*co*-hydroxyvalerate) (PHBV) was developed to achieve a tailored stiffness-toughness balance. The influence of polymer selection, relative ratios, and hybrid compatibilizer addition on blend properties was systematically investigated. Morphological analysis revealed that the blend components remained largely immiscible, consistent with solubility parameter predictions, while interfacial tension measurements indicated that BioPBS effectively separated PHBV and PBAT phases. Optimized ternary blends with 50 wt% PHBV exhibited synergistic mechanical performance, reaching elongation at break close to 100%, tensile strength around 35 MPa, and Young's modulus exceeding 1.6 GPa. Rheological analysis suggested enhanced interfacial interactions due to increased chain entanglement, even in the absence of a compatibilizer. Incorporation of 3–5 wt% hybrid compatibilizer further enhanced mechanical and thermal performance, with elongation at break increasing by 8%, impact strength by 15%, and Young's modulus by 9%, alongside improved thermal stability. These improvements were attributed to interfacial chemical interactions confirmed by Fourier transform infrared spectroscopy, enhanced phase adhesion observed *via* scanning electron microscopy, and more entangled or cross-linked networks indicated by rheology. The results demonstrate that BioPBS/PBAT/PHBV ternary blends can be tailored to produce fully degradable materials with tunable mechanical and thermal properties. Hot melt cast extrusion processing was employed to obtain a cast sheet with high barrier properties, highlighting its potential for sustainable packaging applications.

Received 26th March 2026,
Accepted 4th June 2026

DOI: 10.1039/d6lp00109b

rsc.li/rscapplpolym

1. Introduction

Plastics constitute a critical category of materials due to their low density, high strength-to-weight ratio, and strong resistance to chemical degradation, which makes them vital to modern economies and widely used in almost every aspect of daily life. However, without substantial changes in manufacturing, consumption, and waste management, global plastic waste is projected to reach nearly 12 billion metric tons by 2050, with tens of millions of metric tons already entering the oceans annually and expected to rise sharply.[1] Packaging accounts for roughly 40% of all plastics produced, with 60% of that specifically used for food and beverage applications. Almost all of these packaging materials, around 99%, are made from fossil fuels or newly extracted resources, and most of them are designed to be used only once.[2] Over time, plastics break down into progressively smaller fragments through physical, chemical, and biological processes, eventually reaching sizes at the micrometer or even nanometer scale.[3] This widespread plastic pollution impacts ecosystems and human health across the planet and has even been detected in human blood and placental tissue.[4] It infiltrates water sources, is consumed by plankton, and poses threats to countless species.[5] Although the full extent of microplastic effects is still being studied, their ecological consequences are evident, representing a significant barrier to achieving sustainable development goals.[6]

To mitigate these challenges, sustainable and biodegradable, or degradable, polymers have emerged as potential alternatives. These materials can degrade through chemical and physical processes under specific conditions, offering a solution to the problems associated with landfilling and single-use plastics. Substituting conventional plastics with bio-based and degradable materials at the production stage can significantly reduce greenhouse gas emissions and slow the accumulation of plastic waste.[7] At the end-of-life stage, some

[a]*Bioproducts Discovery and Development Centre, Department of Plant Agriculture, Crop Science Building, University of Guelph, Guelph, N1G 2 W1 Ontario, Canada. E-mail: mohanty@uoguelph.ca, mmisra@uoguelph.ca, mmenossi@uoguelph.ca, manusmriti99@gmail.com, pesarane@uoguelph.ca*
[b]*College of Engineering, Department of Interdisciplinary Engineering, Thornborough Building, University of Guelph, Guelph, N1G 2 W1 Ontario, Canada*
† These authors contributed equally to this work.

bio-based plastics are compatible with existing recycling infrastructures, while others can fully degrade under controlled conditions.[8] Developing these alternatives is therefore urgent.

Degradable polymers, including their blends and composites, represent key solutions for reducing plastic pollution and advancing sustainable materials technologies.[9] Among commercially available degradable polymers, aliphatic polyesters such as poly(butylene succinate) (PBS), poly(3-hydroxybutyrate-*co*-3-hydroxyvalerate) (PHBV), and poly(butylene adipate-*co*-terephthalate) (PBAT), have been known as degradable plastics with a unique property that makes them susceptible to disintegration and decomposition under certain environmental conditions.[10] More specifically, PBS and PBAT have proven biodegradability under industrial compositing, achieving up 90% biodegradation within a maximum of 6 months at 58 °C. In contrast, PHBV, belonging to the polyhydroxyalkanoates (PHAs) family, has the distinct to degrade across a wide range of environments, such as marine environment, freshwater, soil, home and industrial compositing, anaerobic digestion, and landfill conditions.[11] By implementing suitable end-of-life approaches, soil or marine biodegradation, industrial or home-composting, their impact on the environment can be significantly reduced. Advances in technology, combined with decreasing production costs, are making these sustainable polymers increasingly competitive with traditional petroleum-based plastics as viable eco-friendly alternatives. Beyond their degradation capabilities, these polymers also show strong potential for integration into recycling systems through multiple recovery approaches, including enzymatic, chemical, and mechanical recycling methods.[12–15] For example, PBAT/PBS-based blends have been investigated through repeated mechanical recycling, with their chemical and mechanical performance assessed over seven processing cycles.[16] The study found that exposure to high temperatures and shear forces altered the materials' rheological behavior, leading to viscosity changes associated with polymer chain scission and a gradual decline in mechanical performance. However, the blends exhibited better mechanical recyclability compared with degradable polymers, particularly PLA.

It is important to clearly distinguish between key terminology.[17,18] Biopolymers are naturally occurring polymeric substances, such as proteins and polysaccharides, produced by living organisms. These biological systems can also be engineered to synthesize specific polymers, including PHAs, such as PHBV in this study. In contrast, bio-based polymers are derived from renewable feedstocks, typically *via* bio-based monomers such as lactic acid, succinic acid, and ethylene glycol. In this study, PBS is a bio-based polymer, whereas PBAT is primarily fossil-derived. Biodegradable plastics refer to materials that can be broken down by naturally occurring microorganisms, including bacteria, fungi, and algae. More broadly, degradable plastics are designed to undergo significant structural changes under specific environmental conditions, leading to deterioration in their properties over time, as defined by standardized testing protocols relevant to their intended use.

Among these degradable polymers, PBAT has received particular attention as a potential replacement for conventional plastics.[19] Its versatility makes it appropriate for numerous packaging uses, such as garden waste collection bags, food packaging components, and flexible wrapping films. Market demand for PBAT is projected to increase consistently, largely due to rising consumer interest in sustainable packaging solutions and increasingly stringent regulations limiting the use of non-degradable plastics. Despite its biodegradability, PBAT is limited by its lower thermal, mechanical, and barrier performance compared to low-density polyethylene (LDPE); for example, its Young's modulus (E) is only about one-third that of LDPE.[20] These limitations have constrained its broader adoption in packaging applications. In comparison, bio-based PBS (BioPBS), a semi-crystalline aliphatic polyester, offers favorable melt processability comparable to commodity polymers such as polyethylene and polypropylene. BioPBS exhibits relatively high stiffness and thermal resistance, characterized by lower elongation at break (ε_b) than PBAT and a high heat deflection temperature as compared to PBAT and poly(lactic acid) (PLA). Despite these advantages, its applicability in packaging is constrained by insufficient resistance to oxygen and water vapor permeation.[21] To address the complementary shortcomings of PBAT and BioPBS, degradable polymer systems are often engineered through blending with rigid bio-based polyesters to achieve a balanced combination of toughness, stiffness, and thermal performance.[22,23] In this context, PHAs, a family of bio-derived and fully biodegradable polyesters, have attracted significant interest. PHAs are distinguished by their high crystallinity and inherent brittleness, yet their excellent biodegradability and biocompatibility make them compelling candidates for advanced and sustainable material applications.[24] Among the PHA family, PHBV is known for its relatively high barrier performance compared to other biodegradable polymers; however, its brittle nature, limited thermal stability, and higher cost relative to PBAT and BioPBS continue to hinder its widespread adoption.[21]

Collectively, PBAT, PHBV, and BioPBS represent a promising group of degradable polymers for next-generation sustainable materials. While none of these polymers alone satisfies the comprehensive mechanical, thermal, and barrier requirements of commercial packaging, their physicochemical properties are highly complementary.[9] Strategic melt blending of these materials enables precise tailoring of performance attributes, providing a flexible and effective pathway toward application-specific degradable polymer systems.[25] To date, several studies have investigated degradable ternary blends designed to balance limitations and enhance the strengths of individual components, including systems such as PLA/PBS/PBAT,[26,27] PLA/poly(ε-caprolactone) (PCL)/starch,[28–30] PLA/PBS/polyhydroxybutyrate (PHB),[31,32] poly(butylene succinate-*co*-adipate) (PBSA)/PBAT/PHBV,[9] PBAT/PHA/PHBV,[33] PLA/PBS/PHBV,[10] PLA/PBAT/starch,[34] PLA/PHBV/PC.[35] In particular, Zolali and Favis[36] examined interfacial and boundary phase behavior in ternary and quaternary PLA/PBS/PBAT/PHBV blends. However, their investigation was limited to only two PBS/PBAT/PHBV

compositions and involved variations in material suppliers, molecular weights, and the 3-hydroxyvalerate (HV) content of PHBV.

A major challenge in polymer blending is the inherent immiscibility between different polymers. This immiscibility typically drives phase separation, which in turn reduces interfacial adhesion and degrades the mechanical properties of the material.[37] To address this limitation, the incorporation of compatibilizers is a strategy to enhance interfacial interactions and promote phase compatibility, resulting in improved overall material performance.[38] Among these strategies, a common method for producing effective compatibilizers involves grafting polymers with maleic anhydride (MA) *via* reactive extrusion in the presence of an initiator. This process introduces reactive anhydride functionalities along the polymer backbone, which facilitates better interaction between immiscible polymer phases. To date, mostly of MA studies have focused on grafting MA onto individual polymers, such as PHBV,[39] plasticized cellulose acetate,[40] PBSA[41,42] and using these modified materials to improve compatibility in blend systems like PLA-PBAT,[42] PLA-PCL,[43] among other systems.

In contrast, the present approach explores a different strategy, developing an MA-based compatibilizer derived from the same polymer system as the matrix. By retaining structural similarity with the polymer system, this tailored compatibilizer is expected to localize more effectively at the interface, thereby enhancing interfacial adhesion and promoting improved phase integration. McNeil and collaborators[44] developed a hybrid compatibilizer based on PBSA and PBAT and incorporated it at 3 wt% into PBSA-PBAT composites. Their results demonstrated improvements in both mechanical properties and interfacial adhesion within the system. Reports on hybrid or multi-component compatibilizers remain relatively limited in the literature. Wang and Xie[45] introduced a grafted multiphase system, PP-*g*-(MA-styrene (St)), into a ternary polypropylene (PP)/polyamide 6 (PA6)/polystyrene (PS) blend. This compatibilizer improved compatibility among the phases, resulting in finer morphological dispersion and enhanced mechanical properties. Similarly, Li and colleagues[46] developed a multiphase compatibilizer, SEBS-*g*-(MA-*co*-St), using St and styrene-*b*-(ethylene-*co*-butylene)-*b*-styrene (SEBS) for a quaternary blend based on PA6/PS/PP/SEBS. The introduction of this compatibilizer transformed the material behavior from brittle to ductile, enabling tunable morphology and significantly improving overall mechanical performance.

In the present study, BioPBS, PBAT, and PHBV were systematically melt blended across six distinct ratios with the objective of simultaneously achieving high stiffness and toughness. Comprehensive theoretical and experimental analyses were conducted to assess miscibility and phase morphology, constituting the first dedicated and systematic investigation of this specific ternary system. Furthermore, a hybrid compatibilization strategy was implemented by incorporating MA-based compatibilizer compounds with tailored functionality. Accordingly, this work aimed to evaluate the miscibility of BioPBS/PBAT/PHBV ternary blends through an integrated analysis of solubility parameters, interfacial tension, mechanical performance, thermal behavior, rheological response, morphology, and chemical interactions. In addition, the influence of the hybrid compatibilizer at two different loadings was systematically examined. Detailed characterization of the compatibilized blends was ultimately carried out to elucidate structure–property relationships governing the performance of this degradable ternary system. The findings highlight its potential as a sustainable alternative to conventional non-degradable polymers for packaging purposes.

2. Materials & methods

2.1. Materials

In this work, BioPBS (commercial grade FZ71PM) supplied by PTT MCC Biochem Company Limited (Thailand) was utilized. PBAT (grade TH801T) and PHBV with 3 mol% HV (grade ENMAT Y1000P) were obtained from Xinjiang Blue Ridge Tunhe Science & Technology Corporation Ltd and Ningbo Tianan Biologic Materials Co. Ltd (China), respectively. The initiator, Luperox, 2,5-dimethyl-2,5-di(*tert*-butylperoxy)hexane (DHBP) 101 (Lup), was sourced from Arkema. Acetone and MA (purity 99%) were purchased from Fisher Scientific (Canada).

2.2. Methodology

2.2.1. Preparation specimens *via* melt extrusion and injection molding. PHBV, BioPBS, and PBAT pellets were compounded through melt processing in a co-rotating twin-screw extruder (Leistritz, Germany). Before extrusion, the polymers were manually pre-mixed in defined ratios and fed into the extruder hopper. Blending was performed at a feed rate of 6 kg h^{-1} and a screw speed of 100 rpm. A complete overview of the formulations is presented in Table 1, where the samples were identified as BioPBS-PBAT-PHBV-compatibilizer. For example, 30-20-50 represents a blend containing 30 wt% BioPBS, 20 wt% PBAT, and 50 wt% PHBV. Wt% stands for mass percentage.

Two distinct temperature profiles were applied depending on the PHBV content in the formulation. For blends containing a lower proportion of PHBV (samples 40-20-40 and 60-20-20, Table 1), the temperature profile was set to 160/165/165/165/165/165/165/165/165/165/165 °C. In contrast, formulations with higher PHBV content (samples 20-20-60, 10-30-60, 15-25-60, 30-20-50, 30-20-50-3 and 30-20-50-5, Table 1) were processed using a profile of 165/165/165/165/165/165/165/160/155/155/155 °C to maintain stable thermal conditions during extrusion. The extrudate was continuously cooled in a water bath, followed by air drying, and then pelletized using a pelletizer. The resulting pellets were dried overnight in a forced convection oven at 65 °C to reduce moisture content to below 1 wt%.

Mechanical and thermal test specimens were produced from the formulated pellets using a single-screw mini-injection molding machine (MPM Model #55, USA). Injection moulding was conducted using formulation-specific processing conditions. Formulations 40-20-40, 20-20-60, and 60-20-20 were processed at barrel temperatures of 170/186/186 °C (zones 1–3)

Table 1 Summary of polymer formulations, its blends and identifications

Formulation	Concentration (wt%)				Sample ID
	BioPBS	PBAT	PHBV	5%MA + 0.1 phr Luperox	
40%BioPBS/20%PBAT/40%PHBV	40	20	40	—	40-20-40
20%BioPBS/20%PBAT/60%PHBV	20	20	60	—	20-20-60
60%BioPBS/20%PBAT/20%PHBV	60	20	20	—	60-20-20
10%BioPBS/30%PBAT/60%PHBV	10	30	60	—	10-30-60
15%BioPBS/25%PBAT/60%PHBV	15	25	60	—	15-25-60
30%BioPBS/20%PBAT/50%PHBV	30	20	50	—	30-20-50
30%BioPBS/20%PBAT/50%PHBV/3% Hybrid comp	29.1	19.4	48.5	3	30-20-50-3
30%BioPBS/20%PBAT/50%PHBV/5% Hybrid comp	28.5	19.0	47.5	5	30-20-50-5
Neat PHBV	—	—	100	—	PHBV
Neat BioPBS	100	—	—	—	BioPBS
Neat PBAT	—	100	—	—	PBAT

with injection pressures of 450/350/250 psi. Formulations 10-30-60 and 15-25-60 employed lower temperatures (170/175/175 °C) and higher pressures (600/450/300 psi), while formulation 30-20-50 used the same temperature profile with reduced pressures (450/350/250 psi). Progressive reductions in pressure were applied for formulations 30-20-50-3 (400/300/200 psi) and 30-20-50-5 (350/250/150 psi) at 170/175/175 °C. Formulation PHBV was processed at 165/170/170 °C with pressures of 550/450/350 psi, whereas formulation BioPBS required lower temperatures (145/150/160 °C) and moderate pressures (500/400/300 psi). The highest temperature and pressure conditions were applied to formulation PBAT (175/180/180 °C; 850/600/450 psi). For the neat polymers (BioPBS, PBAT, and PHBV), the pellets were directly fed into the injection molding machine without pre-blending. The specimens for mechanical testing were prepared according to the dimensional requirements of relevant ASTM standards: D638-14 (Type IV) for tensile testing, D790-17 for flexural testing, and D256-10 for notched Izod impact testing.

2.2.2. Hybrid compatibilizer preparation. Among the ternary blend formulations, one composition was selected based on its superior mechanical properties. To enhance interfacial compatibility within this blend, a hybrid grafting approach incorporating MA and Lup was employed, following the methodology reported by Garcia-Castellanos *et al.*[47] Briefly, 1 parts per hundred (phr) of Lup was first added to the selected formulation and uniformly mixed with the polymer pellets. This was followed by the addition of 5 wt% MA, and the mixture was stirred for approximately 2 minutes. The modified blend was subsequently processed using a twin-screw extruder operated under a temperature profile of 155/165/165/165/165/165/165/160/155/155/155 °C, with a feed rate of 5 kg h^{-1}. A reduced screw speed was used to increase the material's residence time within the barrel, facilitating effective grafting. The resulting extrudates were subsequently passed through a water-cooling bath and converted into pellets.

2.3. Characterization

2.3.1. Characterization of the hybrid compatibilizer. Fourier transform infrared (FTIR) spectroscopy (Nicolet Summit X, Thermo Scientific) was used to verify MA grafting onto the BioPBS-PBAT-PHBV blend. The measurements were performed using 4 cm^{-1} as a resolution and 32 consecutive scans. As a result of MA incorporation along the BioPBS/PBAT/PHBV backbone, the FTIR spectra displayed one additional absorption peaks in 1780 cm^{-1} that were absent in the neat BioPBS-PBAT-PHBV sample (Fig. S1, SI), as we already report in another work related to meleation of PHBV.[39] The grafting level was quantified through an acid–base titration method, yielding a MA grafting percentage of 1.89 ± 0.17% for MA-grafted-BioPBS-PBAT-PHBV blend (30-20-50 wt%); the detailed titration procedure is available in our earlier publication.[41]

2.3.2. Contact angle measurements and interfacial tension. Contact angle measurements were conducted on extruded samples using a Ramé-Hart standard goniometer (Model 260-U1) composed solely of neat PBAT, BioPBS, or PHBV. The static sessile drop method was employed, in which droplets of test liquids were dispensed onto the sample surface using a microsyringe. Tests were carried out at ambient temperature (~20 °C) using injection-molded specimens. Deionized water and diiodomethane were selected as the polar and non-polar probe liquids, respectively. The surface free energies and their components for each liquid are summarized in Table S1 (SI), with the dispersive (γ^d) and polar (γ^p) components of surface tension for each liquid.[48] Contact angles were analyzed using DROPimage software (version 2.8.05). Additionally, the surface tension values of the neat polymers were computed using the same software, based on both the harmonic and geometric mean methods. For each polymer, measurements were taken at three different positions, and all tests were performed in triplicate. The results are summarized as average values accompanied by standard deviations.

The surface tensions of the three polymers were estimated based on the measured contact angles using Young's equation (eqn (1)):[49]

$$\gamma_s = \gamma_{sl} + \gamma_l \cos\theta \quad (1)$$

In this context, γ_s and γ_l correspond to the surface tensions at the solid–vapor and liquid–vapor interfaces, respectively, while γ_{sl} refers to the interfacial tension between the solid and

liquid phases; θ denotes the contact angle. To enable a more detailed evaluation of surface energy characteristics, the Owens–Wendt–Rabel–Kaelble (OWRK) method was employed.[50] This approach separates the total surface energy into dispersive and polar contributions, which collectively define the overall surface tension of the material. The OWRK model provides a more detailed way to describe how solids and liquids interact at their interface, as shown in eqn (2):

$$\gamma_l(1+\cos\theta) = 2\left(\sqrt{\gamma_s^d\gamma_l^d} + \sqrt{\gamma_s^p\gamma_l^p}\right) \quad (2)$$

In this equation, the superscripts d and p denote the dispersive and polar components of surface tension, respectively, and θ represents the contact angle measured in radians. By combining experimentally obtained contact angles for two probe liquids with their known total surface tensions and corresponding component values (γ_l, γ_l^d, and γ_l^p), see Table S1 (SI), eqn (2) generates a system of two simultaneous equations with two unknown parameters (γ_s^d and γ_s^p). Solving this system allowed the individual surface energy components to be quantified, and their sum ($\gamma_s = \gamma_s^d + \gamma_s^p$) was calculated for each polymer sample.

To further understand the interfacial interactions and predict the likely morphology of the blends, the interfacial tensions between each pair of polymers were estimated. Two theoretical models were employed for this purpose: the harmonic mean method and the geometric mean method,[51] as we already explained in our previous work.[48]

2.3.3. Solubility parameter calculations. To assess the miscibility of the ternary blend, solubility parameters (δ) for each polymer were sourced from published data to facilitate comparison. This parameter reflects the internal cohesive forces of materials and serves as a reliable predictor of miscibility in polymer-solvent systems.[52] The original concept of solubility behavior was introduced by Hildebrand, later enhanced by Hansen through the division of the solubility parameter into three components: dispersive, polar, and hydrogen bonding.[53] The Hansen solubility parameters can be estimated using the Hoftyzer–van Krevelen group contribution method, which calculates values based on the chemical structure of the polymer.[54] In this study, this method was employed to estimate the difference of δ ($\Delta\delta$) of the polymers involved. It entails adding the contributions of functional groups within the polymer chains to determine each of the three components. The number of repeating units in each polymer was determined using the average molecular weight (M_w) of the respective materials. The M_w values for PBAT, BioPBS, and PHBV were 18 000,[23] 18 600,[55] and 240 000 g mol^{-1},[56] respectively.

2.3.4. Mechanical properties. Flexural and tensile characterization was carried out using an Instron 3382 universal testing system (MA, USA) in accordance with the applicable ASTM protocols outlined in section 2.2.1. Tensile experiments were conducted at a crosshead rate of 50 mm min^{-1} for all formulations; however, neat PHBV and PBAT were tested at 5 mm min^{-1} and 500 mm min^{-1}, respectively, to account for their distinct deformation responses. Instron 3382 was equipped with a 5 kN cell load for all measurements. Flexural measurements were performed with a support span of 52 mm and a loading rate of 14 mm min^{-1}. The notched Izod impact strength was measured with a ZwickRoell impact testing machine. A minimum of five specimens were analyzed for each test, and the data are presented as average values accompanied by standard deviations.

2.3.5. Thermal analysis

2.3.5.1. Differential scanning calorimetry (DSC). The thermal behavior of the compounded pellets was characterized with a Differential Scanning Calorimeter (DSC) Q200 manufactured by TA Instruments (New Castle, USA). The study focused on identifying the blends' thermal transitions, including melting and crystallization behaviors, glass transition temperatures (T_g), and the associated enthalpy changes. Approximately 8–10 mg of each sample was used per measurement. The testing protocol consisted of an initial heating stage from ambient temperature up to 200 °C at a heating rate of 10 °C min^{-1}, after which the materials were cooled to −70 °C at 5 °C min^{-1}. A second heating scan was then carried out up to 200 °C using the same 10 °C min^{-1} rate. Crystallization temperatures and enthalpy values were extracted from the cooling cycle, whereas melting characteristics were determined from the second heating run. The crystallinity fraction (X_c) was determined using eqn (3):

$$X_c(\%) = \frac{\Delta H_m}{\Delta H_m^\circ \times W_p} \times 100\% \quad (3)$$

where ΔH_m represents the experimentally measured melting enthalpy, W_p corresponds to the polymer weight fraction in the blend, and ΔH_m° denotes the melting enthalpy of a 100% crystalline polymer. Reference values of 200 J g^{-1} for PBS[57] and 146 J g^{-1} for PHBV[58] were used in the calculations.

2.3.5.2. Thermogravimetric analysis (TGA). Thermal stability measurements were carried out with a TGA Q500 thermogravimetric analyzer (TA Instruments, New Castle, USA). For each measurement, approximately 10–15 mg of sample, taken from sections of extruded strands or pellets, was used. The specimens were subjected to heating from ambient temperature up to 600 °C at a uniform heating rate of 10 °C min^{-1} under a nitrogen (N_2) environment to minimize oxidative effects.

2.3.6. Scanning electron microscopy (SEM). The morphological features of the fractured surfaces were investigated using a scanning electron microscope (SEM; Quanta FEG 250, Thermo Fisher Scientific) operated at an accelerating voltage of 20 kV. Fracture surfaces were taken from impact-tested specimens and imaged at a magnification of 5000×. Prior to imaging, a thin gold coating was applied using a sputter coater to enhance resolution and minimize surface charging. The coating was applied at 20 mA for 90 s, resulting in an approximate thickness of 8 nm.

To further examine the internal structure, a selective etching procedure was conducted. Tetrahydrofuran (THF) was used to dissolve the PBAT phase, with samples immersed in THF for 3 minutes, followed by thorough rinsing with deionized water. The specimens were dried completely before SEM analysis. These images were examined using a Phenom ProX scanning electron microscope (Phenom-World, Netherlands) operated at an accelerating voltage of 10 kV at magnifications of 5000× and 10 000×.

2.3.7. Fourier transform infrared spectroscopy (FT-IR). Fourier-transform infrared (FTIR) analysis was carried out on a Nicolet Summit X spectrometer (Thermo Scientific) to characterize the chemical structure of the samples through identification of their principal functional groups. Spectral data were obtained under room-temperature conditions using an attenuated total reflectance (ATR) accessory configured for transmission measurements. Infrared spectral measurements were collected between 600 and 4000 cm^{-1} using a spectral resolution of 4 cm^{-1}. To improve the signal-to-noise performance, each reported spectrum was generated by averaging 32 individual scans.

2.3.8. Rheological studies. The flow and viscoelastic properties of the unmodified polymers and their blends were characterized under a N_2 environment using a rotational rheometer (MCR 302, Anton Paar, Germany) fitted with a 25 mm parallel-plate geometry and a 1 mm gap. All tests were performed at 175 °C, which corresponds to the maximum temperature employed during injection moulding. Dynamic oscillatory testing was performed using a constant strain of 1%, while the frequency was varied from 100 to 0.01 Hz to characterize the rheological behavior of the materials.

2.4. Blend cast sheet extrusion

The formulation identified as optimal from mechanical properties evaluation was processed into cast sheets using a cast film extrusion setup (Microtruder RCP-0625, Randcastle, USA) fitted with a 1.25 in single-screw extruder featuring a 24 : 1 L/D ratio, along with a slit die and chill roll assembly. Processing was performed under a temperature sequence of 175, 175, 180, 185, and 185 °C across extrusion zones 1–4 and the die, respectively. Throughout extrusion, the screw rotation speed was fixed at 30 rpm, whereas the take-up rolls operated at 15 rpm. The slit die opening was calibrated to obtain sheets with a mean thickness close to 0.25 mm.

2.4.1. Mechanical properties. The tensile behavior of the prepared films was evaluated along the machine direction in accordance with ASTM D882-18. Measurements were carried out at room conditions using an Instron 3382 universal testing system (Massachusetts, USA) fitted with a 5 kN load cell and operated through Bluehill software. Test parameters, including crosshead velocity, gauge distance, and specimen dimensions, were determined according to the expected ε_b specified in ASTM D882-18. A total of ten specimens were analyzed for each formulation.

2.4.2. Barrier properties. The moisture barrier characteristics of the developed films, including Water Vapor Transmission Rate (WVTR) and Water Vapor Permeability (WVP), were evaluated with a MOCON Permatran-W 3/33 instrument following the ASTM F1249 standard under conditions of 90% relative humidity and 37.8 °C. Circular film samples with a test area of 5 cm^2 were clamped between aluminum holders and installed in a two-compartment permeation cell. N_2 of high purity was introduced at a constant flow rate of 100 cm^3 min^{-1}. As moisture diffused across the film matrix, the transported water vapor was swept by the N_2 carrier gas toward the detection system, enabling determination of the film's WVP.

Oxygen Transmission Rate (ORT) and Oxygen permeability (OP) was measured using a Mocon OX-TRAN 2/21 analyzer (USA) following ASTM D3985 at 0% RH and 25 °C. Samples of similar dimensions were analyzed, and a nitrogen carrier gas flow of 10 cm^3 min^{-1} was used to transport oxygen molecules permeating through the film to the detector. The detected oxygen transmission was subsequently used to calculate the OP values. Two specimens were analyzed for each test.

3. Results and discussion

3.1. Contact angle measurements and interfacial tension

The wettability evaluation is used to understand how a liquid behaves when in contact with a solid surface. When the interaction between the two is strong, the contact angle decreases, leading to reduced interfacial tension and improved liquid penetration into the polymer structure.[59] Surface wettability plays a key role in defining the material's response to fluid exposure. Materials that are hydrophobic, typically non-polar and resistant to water, tend to repel moisture. In contrast, if the contact angle formed by a droplet on the surface is below 90°, the surface is considered hydrophilic; if it exceeds 90°, the material is classified as hydrophobic.[60]

To evaluate the surface wettability of the individual polymers, PBAT, BioPBS, and PHBV, contact angle measurements using water and diiodomethane were performed on their molded samples. The corresponding data are compiled in Table 2. Representative images illustrating the contact angles for both liquids on these neat polymer surfaces can be found in the Fig. S2 (SI). Among the tested polymers, BioPBS and PBAT showed the highest contact angles for both water and diiodomethane, measuring 73.0° and 71.1° for water, and 45.9° and 42.2° for diiodomethane, respectively (Table 2). In contrast, PHBV displayed the lowest contact angles, with both values recorded at 68.3°. These findings suggest that all three polymers demonstrate a relatively hydrophilic surface character rather than hydrophobic, aligning with previous literature reports on PHBV,[61] PBAT,[62] and BioPBS.[27] In agreement with these results, PHBV exhibits the highest surface tension, which corresponds to the lowest wettability and indicates weaker solid–liquid interactions with the probing liquids (Table 2).

The morphology of ternary polymer blends can often be anticipated using the concept of the spreading coefficient,

Table 2 Contact angle measurements and calculated total surface tension (γ), including its polar (γ^p) and dispersive (γ^d) components, for the three individual polymers

			Surface tension (mN m^{-1})					
	Contact angle (°)		Harmonic mean			Geometric mean		
Polymer	Water	Diiodomethane	γ^p	γ^d	γ^{total}	γ^p	γ^d	γ^{total}
PHBV	68.3 ± 0.8	40.7 ± 0.3	13.8	39.9	53.6	8.3	39.3	47.6
BioPBS	73.0 ± 4.3	45.9 ± 1.4	12.1	37.4	49.5	7.0	36.5	43.5
PBAT	71.1 ± 2.6	42.2 ± 0.6	12.6	39.1	51.7	7.3	38.5	45.7

originally introduced by Harkins,[63] since interfacial tension thermodynamically governs the structural arrangement in polymeric systems.[64] This approach distinguishes two primary wetting scenarios, complete wetting and partial wetting, that have been observed and accurately described through the spreading coefficient model. For ternary polymer blends, Harkins' expression is adapted, as shown in eqn (4):

$$\lambda_{ij} = \gamma_{jk} - \gamma_{ik} - \gamma_{ji} \quad (4)$$

In this context, k denotes the polymer matrix, while λ_{ij} represents the spreading coefficient of component i over component j. Based on spreading coefficient principles, thermodynamic encapsulation of j by i occurs when λ_{ij} is positive and λ_{ji} is negative, leading to the formation of a core–shell (j–i) morphology.[65] Alternatively, when both coefficients are negative, component i preferentially wets the interface between k and j, provided that λ_{ki} or λ_{kj} is also negative.[36] In contrast, if λ_{ij} and λ_{ji} are both negative while λ_{ki} or λ_{kj} is positive, components i and j are expected to remain as distinct dispersed phases within matrix k.[66]

Analysis of interfacial tension values for the BioPBS-PBAT-PHBV ternary system reveals that the PHBV-PBS pair exhibits lower interfacial tension (0.11 and 0.21 mN m^{-1} using harmonic and geometric means, respectively) compared with PBS-PBAT (0.02 and 0.05 mN m^{-1}) and PHBV-PBAT (0.03 and 0.07 mN m^{-1}), indicating comparatively stronger interfacial affinity between PHBV and PBS. Due to the lowest free energy principle in the multi-component system and the positive value of the $\lambda_{PBAT/PBS}$ (Table 3) spreading coefficient suggests a complete wetting behavior, when the polymeric matrix is BioPBS (samples 40-20-40 and 60-20-20, Table 1), it appears that BioPBS exhibits complete wetting behavior, fully separating the PHBV and PBAT phases from each other. Zaloli and Favis[36] examined the phase morphology of polymer blends consisting of PHBV, PBAT, PBS, and PLA through spreading coefficient calculations, SEM, and atomic force microscopy (AFM). At low PBAT concentrations, they found that PBAT formed partially wetted droplets positioned at the interface between PBS and PHBV, which remained stable even after quiescent annealing. However, when the PBAT content was increased to 25 wt%, it initially created a continuous phase during mixing. This structure later transformed into partially wetted PBAT droplets only after thermal annealing. When PHBV is the polymeric matrix, λ_{ij} is positive, λ_{ji} is negative and both λ_{ki} and λ_{kj} are negatives, adopting a core–shell configurations (samples 20-20-60, 10-30-60, 15-25-60, 30-20-50, 30-20-50-3 and 30-20-50-5). Further details and clarification of these morphological behaviors are discussed in section 3.5.

It is important to note that Zaloli and Favis[36] employed a PHBV grade containing approximately 8 mol% HV, which is nearly double the HV content of the PHBV used in the present study. An increase in HV content is known to reduce crystallinity and increase the amorphous fraction of PHBV. Because amorphous domains are more accessible to water molecules and polar interactions than crystalline regions, higher HV contents are commonly associated with an increase in the apparent polarity of PHBV. In agreement with this interpretation, Abate *et al.*,[67] reported that PHBV with higher HV content exhibits reduced solubility in organic solvents compared to low-HV PHBV.

3.2. Solubility parameters

The δ for PHBV and PBAT based on Hoy, Hoftyzer–Van Krevelen, and Hansen methods were sourced from previously published literature.[23,56] In contrast, for BioPBS, the Hansen solubility parameter was adopted from the work of Patel *et al.*,[55] while the Hoy and Hoftyzer–Van Krevelen values were newly calculated in the present study. A summary of δ values is provided in Table 4.

Table 3 Extrapolated interfacial tension and spreading coefficient at 20 °C and 160 °C using harmonic and geometric mean approaches

				Spreading coefficient (mN m^{-1})					
	Interfacial tension 20 °C (mN m^{-1})			20 °C			160 °C		
Equation	$\gamma_{PHBV/PBS}$	$\gamma_{PBS/PBAT}$	$\gamma_{PHBV/PBAT}$	$\lambda_{PHBV/(PBS\ or\ PBAT)}$	$\lambda_{PBS/PBAT}$	$\lambda_{PBAT/PBS}$	$\lambda_{PHBV/(PBS\ or\ PBAT)}$	$\lambda_{PBS/PBAT}$	$\lambda_{PBAT/PBS}$
Harmonic	0.11	0.02	0.03	−0.12	−0.10	0.06	−0.13	0.05	−0.12
Geometric	0.21	0.05	0.07	−0.24	−0.19	0.10	−0.28	0.11	−0.21

Table 4 Hoftyzer–Van Krevelen, Hoy, and Hansen parameters (δ) of neat polymers, PHBV, PBAT, and BioPBS

Compound	Hoftyzer–Van Krevelen	Hoy	Hansen	Average
BioPBS	22.1	18.4	20.7[55]	20.4
PHBV[56]	19.9	21.6	20.6	20.7
PBAT[23]	22.8	20.8	20.7	21.5

The δ offers valuable insight into the cohesive intermolecular forces, specifically polar interactions, dispersion forces, and hydrogen bonding, which collectively influence the miscibility of polymer components. Both the Hoftyzer–Van Krevelen and Hoy methods are commonly used to estimate δ by accounting for these interactions.[54] The Hoftyzer–Van Krevelen method calculates δ based on the group contribution approach, emphasizing the roles of polar and hydrogen bonding groups. Conversely, the Hoy method incorporates additional correction factors to better reflect molecular non-ideality and aggregation effects.

According to Forster *et al.*[68] a $\Delta\delta$ of less than 2.0 $MPa^{1/2}$ suggests good miscibility, while values exceeding 10.0 $MPa^{1/2}$ indicate immiscibility. Based on this guideline, the three degradable polymers examined in this study appear to be theoretically miscible. Consequently, these blends are likely suitable for processing *via* extrusion followed by injection molding; however, experimental validation is necessary to confirm the actual degree of miscibility.

3.3. Mechanical properties

Mechanical behaviour of the Bio-PBS-PBAT-PHBV blend and the neat polymers was studied *via* tensile, flexural, and impact testing. The results are summarized in Fig. 1. As can be seen in this figure, the neat polymers are demonstrating very different mechanical performance. PHBV shows the highest tensile/flexural strength and modules while it indicates low ε_b and impact resistance. On the other hand, PBAT shows the characteristics of an elastomer with high ε_b and superior resistance against impact, while it shows the lowest stiffness in terms of tensile/flexural modulus among the three degradable polymers. BioPBS demonstrates a balanced mechanical performance with intermediate values of modulus, ε_b and tensile strength (σ). The mechanical results obtained for the neat polymers agree with previously reported data.[22,23]

Melt blending of degradable polymers with complementary mechanical properties could help reach a balance of performance. Such a capacity of the melt blending approach could also be observed in the results of this study. First, we can compare the blends 20-20-60, 10-30-60, and 15-25-60, which contain the highest level of high-stiffness PHBV as the main component of the blend (60 wt%). As can be observed, the mechanical performance of these blends is highly affected by the ratio of the two other components, BioPBS and PBAT. According to the mechanical analysis, highly flexible PBAT is more effective in enhancing the impact resistance in these ternary blends (Fig. 1c), while the ε_b did not show high dependence on the weight ratio between BioPBS and PBAT. Accordingly, while ternary blends 20-20-60 and 15-25-60 showed very similar impact resistance (28.2 and 25.7 J m^{-1}) to neat PHBV (26.8 J m^{-1}), the impact strength was increased significantly in ternary blend 10-30-60 (52.2 J m^{-1}) with the highest level of PBAT (30 wt%). Despite this improvement in impact strength, blend 10-30-60 shows lower σ and E, which is a direct result of the presence of PBAT with low stiffness and strength. The incompatibility between PHBV as the matrix of the blend and both PBAT and BioPBS could result in a weak interfacial attraction between the matrix and dispersed phases. In such conditions, melt blending of a highly flexible PBAT or BioPBS could not help enhancing the ε_b of PHBV. However, the debonding of the dispersed phase from the matrix can act as a toughening mechanism during the impact test. In fact, the debonding between matrix and dispersed phase could trigger shear deformation within the matrix, which is known as an energy-absorbing mechanism, and consequently, results in improved impact strength of the blend.[10]

At the fixed concentration of PBAT at 20 wt% (samples 40-20-40, 20-20-60, 60-20-20, and 30-20-60), the mechanical performance of the ternary blend is controlled by the weight ratio of two other components, BioPBS and PHBV. Clearly, a transition from ductile to brittle behavior is observed when the content of PHBV reaches 50 wt% and more in blends 30-20-50 and 20-20-60, while blend 60-20-20 with the lowest content of PHBV (20 wt%) is showing the highest level of both ε_b (189%) and impact strength (49.7 J m^{-1}). On the other hand, by increasing the content of PHBV, both σ and E and flexural modulus indicate improvement (Fig. 1a and b).

Based on the mechanical testing conducted in this study (Fig. 1d), sample 30-20-50 was selected for further development using a compatibilization strategy. This selection was driven by the potential of PHAs to access new markets, as well as their inherent biodegradability. PHAs are biodegradable polymers and are among the few biopolyesters that readily degrade across a wide range of environments, including marine and freshwater systems, soil, and compost. In contrast, BioPBS and PBAT primarily degrade under industrial composting conditions at controlled temperatures; PBAT may exhibit home-compostability or soil biodegradability only under specific conditions or for certain grades.[11] Under these circumstances, PHAs represent a particularly promising bio-based polymer for packaging applications. Accordingly, material development efforts, such as improving mechanical performance through compatibilization, should be prioritized for this system.

MA grafted polymers are commonly used in degradable polymer blends to enhance the compatibility between immiscible polymers and consequently enhance the mechanical performance of the final blend.[39] A similar approach was adopted in this study by synthesizing a hybrid compatibilizer and incorporating it into blend 30-20-50 at two different concentrations. A slight improvement was observed in E and ε_b for blends 30-20-50-3 and 30-20-50-5, which contained 3 and 5 wt% hybrid compatibilizer, respectively. Specifically, the addition of 3 and

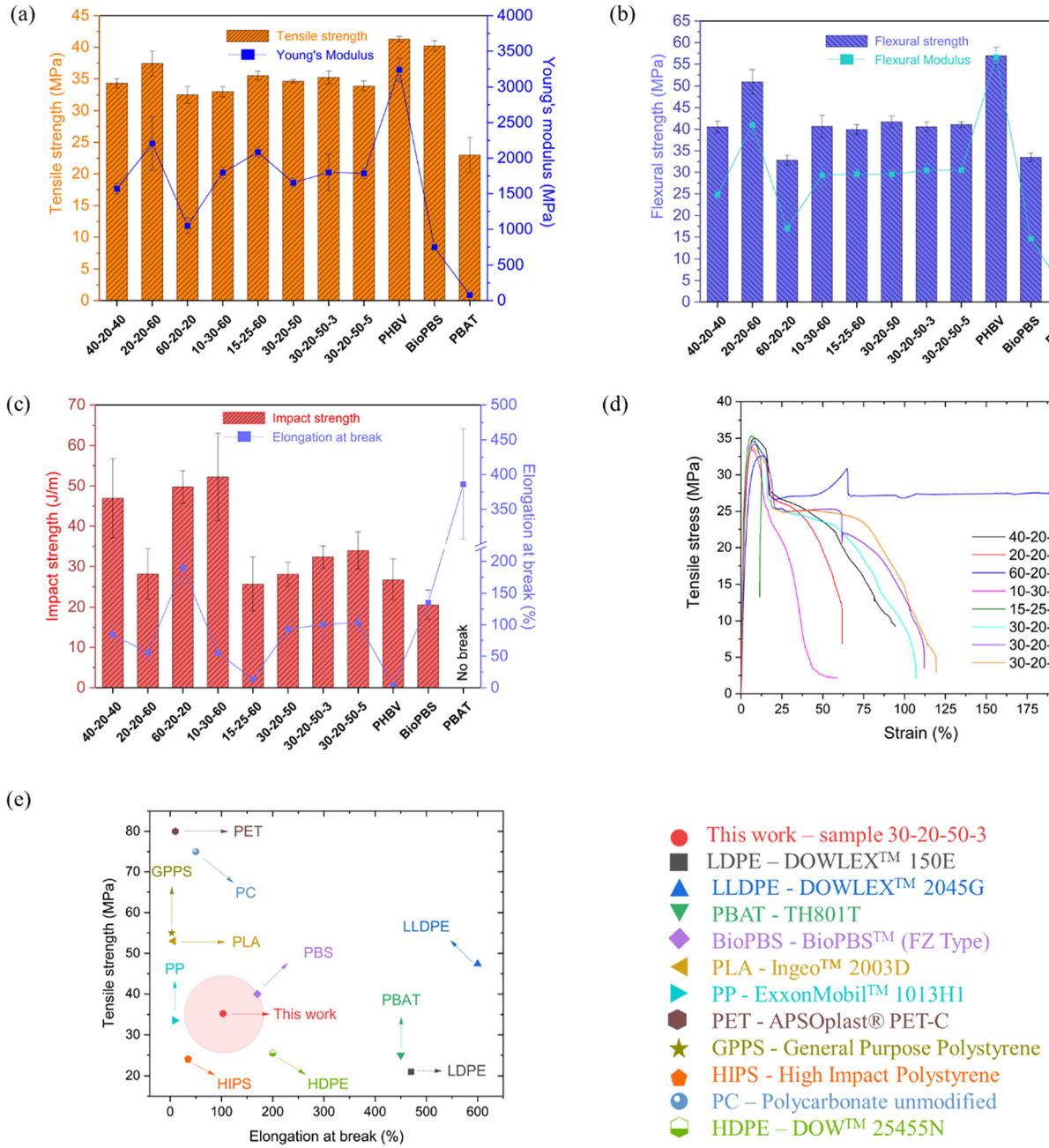

Fig. 1 Mechanical properties of the ternary blends and neat polymers: (a) tensile strength and modulus; (b) flexural strength and modulus; (c) elongation at break and notched Izod impact strength; (d) representative stress–strain curve for each sample; and (e) mechanical properties comparison. The samples were identified as BioPBS-PBAT-PHBV-compatibilizer. LDPE, LLDPE, and HDPE/https://www.dow.com/en-us (accessed on May 7th, 2026); PBAT/https://pycnoplast.com/wp-content/uploads/2023/05/PBAT-TH801-TDS.pdf (accessed on May 7th, 2026); PBS/https://www.pttmcc.com/file_upload/tds/TDS-FZ71PM_PB.pdf (accessed on May 7th, 2026); PLA/https://natureworksllc.com (accessed on May 7th, 2026); PP/https://www.exxonmobilchemical.com/en (accessed on May 7th, 2026); PC/https://plastim.co.uk/ (accessed on May 7th, 2026); HIPS and GPPS https://plaskolite.com/ (accessed on May 7th, 2026).

5 wt% compatibilizer increased the ε_b by approximately 8% and 11%, respectively. Furthermore, the impact strength also improved upon compatibilizer addition, as shown in Fig. 1, reaching an increase of approximately 21% at 5 wt% hybrid compatibilizer. As discussed, the localization of the compatibilizer at the interface between the PHBV matrix and the dispersed phases likely enhances interfacial adhesion, could be attributed to the observed improvements in mechanical properties. Similar effects have been reported by other authors,[47] who demonstrated that the addition of MA, based compatibilizers can improve interfacial interactions in multiphase polymer systems.

Conventional packaging materials are largely derived from persistent, non-biodegradable polymers. These typically comprise polyethylene-based resins such as high-density polyethylene (HDPE), low-density polyethylene (LDPE), and linear low-density polyethylene (LLDPE), along with polypropylene (PP), polyethylene terephthalate (PET), polycarbonate (PC), and polystyrene materials including general-purpose polystyrene (GPPS) and high-impact polystyrene (HIPS). In contrast, the primary degradable polymers being explored as alternatives to conventional plastics are PBAT, PBS, and PLA. Fig. 1e illustrates the wide variation in their mechanical performance, including the best mechanical performance in this study (30-20-50-3), particularly in terms of σ and ε_b. In general, flexible packaging application is characterized by relatively low σ with an exceptional high ε_b, as LDPE and PBAT. The more linear molecular structure of LLDPE contributes to higher σ while maintaining favorable ε_b properties. In contrast, rigid or stiff packaging materials such as PLA, PP, PC, GPPS, HIPS, and PET typically display comparatively higher σ but substantially lower ε_b values. Compared with these materials, the optimized formulation developed in this work demonstrates σ and ε_b values like those of neat PBS, while achieving more than twice the E (Fig. 1a).

3.4. Thermal analysis

DSC was utilized to qualitatively analyze the thermal behavior of the samples, with the results summarized in Table 5 and Fig. S3 (SI) shows heat and cool cycles for each sample. The cooling cycle provided insights into the crystallization temperature (T_c) and its corresponding enthalpy (ΔH_c). Meanwhile, the second heating cycle revealed data on melting temperatures (T_m) and associated enthalpies (ΔH_m). In the subsequent heating scan, the thermogram displayed two separate endothermic transitions. he lower-temperature transition, corresponded to the melting of BioPBS and potentially PBAT around 114 °C, while the second was attributed to the melting of PHBV around 171 °C. The cooling cycle also reveals two crystallization peaks, one at the range of 70–80 °C corresponding to BioPBS, and the other one at higher temperatures (95–110 °C), corresponding to the PHBV. Analysis of the melting and crystallization behavior of PHBV in the various blends indicated no significant changes in its T_m, T_c, or X_c. The only notable deviation was observed in blend 60-20-20, which contained the lowest PHBV content. The reduction in the T_c of PHBV in this blend may be attributed to crystallization occurring in the presence of molten BioPBS. Specifically, the molten BioPBS phase may hinder the diffusion of PHBV macromolecules toward growing crystals, thereby lowering the crystallization temperature. Nevertheless, the overall crystallinity of PHBV remained essentially unchanged across all blends. For BioPBS, no significant variations in T_c, T_m, or X_c were observed among the different blends. Overall, variations in the relative amounts of the ternary components did not significantly influence the thermal behavior of the system. Similar behavior was reported by Hedrick and colleagues,[35] who investigated the thermal properties of degradable ternary

Table 5 Differential scanning calorimetry for the neat ternary blend and its composites

	BioPBS					PHBV				
Sample	T_g [°C]	T_m [°C]	ΔH_m [J g^{-1}]	x_c [%]	T_c [°C]	ΔH_c [J g^{-1}]	T_m [°C]	ΔH_m [J g^{-1}]	x_c [%]	T_c [°C]	ΔH_c [J g^{-1}]
40-20-40	−30.1 ± 0.2	114.9 ± 0.1	35.8 ± 5.6	44.8 ± 7.0	79.1 ± 0.5	35.5 ± 1.3	170.9 ± 0.1	37.0 ± 2.0	63.4 ± 3.5	103.9 ± 0.1	40.1 ± 0.6
20-20-60	—	113.6 ± 0.1	23.9 ± 1.3	59.7 ± 3.2	75.8 ± 0.1	14.3 ± 2.5	168.8 ± 0.1	48.1 ± 3.9	54.9 ± 4.5	106.5 ± 0.1	56.9 ± 2.2
60-20-20	−28.7 ± 4.5	114.2 ± 0.5	56.5 ± 3.6	47.1 ± 3.0	74.4 ± 2.3	50.2 ± 1.1	168.8 ± 1.1	18.5 ± 1.1	63.3 ± 3.8	94.1 ± 3.2	6.0 ± 0.6
10-30-60	—	113.5 ± 0.1	8.5 ± 1.7	42.4 ± 8.7	78.8 ± 0.9	2.7 ± 0.2	170.9 ± 0.2	53.5 ± 2.0	61.1 ± 2.3	108.1 ± 0.1	65.1 ± 1.5
15-25-60	—	113.1 ± 0.4	11.8 ± 0.1	39.4 ± 0.4	—	—	169.4 ± 0.8	52.3 ± 0.7	60.7 ± 0.8	108.6 ± 0.2	70.4 ± 3.9
30-20-50	−28.1 ± 3.1	114.5 ± 0.2	26.0 ± 4.3	43.3 ± 7.1	80.1 ± 0.2	29.0 ± 5.7	171.2 ± 0.1	45.2 ± 6.7	61.9 ± 9.2	106.0 ± 0.6	59.5 ± 7.1
30-20-50-3	−32.4 ± 2.8	114.1 ± 1.0	20.0 ± 5.4	34.4 ± 9.3	81.3 ± 4.9	18.7 ± 6.5	169.9 ± 2.0	43.9 ± 4.4	62.0 ± 6.2	106.8 ± 1.0	54.3 ± 3.5
30-20-50-5	−31.4 ± 1.7	113.9 ± 0.4	23.3 ± 5.7	40.9 ± 10.0	78.7 ± 4.1	22.2 ± 2.2	169.6 ± 1.2	44.2 ± 0.8	63.7 ± 1.2	106.0 ± 0.4	53.3 ± 1.4

blends based on PLA, PHBV, and polypropylene carbonate (PPC). They observed a slight decrease in PHBV crystallinity, which was attributed to the amorphous nature of PPC hindering PHBV crystal growth. When sufficient chain and interfacial mobility is available, as observed in certain ternary systems,[10] PHBV can serve as an effective nucleating agent to promote polymer crystallization. In this context, interfacial characteristics play a critical role in governing nucleation efficiency.[35] Consequently, the nature of phase interfaces must be carefully considered when evaluating crystallization kinetics in melt-blended polymer systems.[69,70] Differences in terminal group chemistry and bulk polymer functionality, particularly in systems containing small molecules with a high density of short chain ends, can enhance chain mobility and interfacial orientation, thereby facilitating localized alignment and subsequent crystalline development.[70–72]

The thermal stability of the blends was evaluated using TGA, and the corresponding results, including the maximum degradation temperature (T_{max}) of the neat polymers and their blends, are summarized in Table 6 and the weight and derivate weight loss *vs.* temperature of each sample is shown in Fig. S4a and b (SI). Neat PBAT and BioPBS showed a very similar T_{max} (408.8 and 410.4 °C), implying similar thermal stability of these two polymers.[23,73] On the other hand, the PHBV with lower T_{max} (303.1 °C) indicated lower thermal stability, as already reported in the literature.[58] The ternary blends displayed two distinct degradation peaks: the lower T_{max} was associated with the PHBV phase, while the higher T_{max} corresponded to the PBAT and BioPBS components. Notably, the melt-blending process did not significant affect the thermal stability of the individual polymers, as evidenced by the negligible changes in T_{max} values of the blends relative to those of the neat materials. However, sample 30-20-50 exhibited a reduction in T_{max} of approximately 10 °C compared to the other samples. This behavior may be attributed to the decreased PBAT and increased BioPBS content in this formulation, which likely reduced the formation of a protective char layer from PBAT.[74] Such a char layer can temporarily act as a thermal barrier, delaying PHBV degradation as the temperature increases.

Additionally, TGA was employed to evaluate the influence of hybrid compatibilization on the thermal stability of the blends at two loading levels, 3 and 5 wt% (samples 30-20-50-3 and 30-20-50-5). Notably, even at the lower loading level, the $T_{5\%}$ increased by nearly 20 °C, rising from 274.5 °C to 295.9 °C. This pronounced enhancement, together with the observed improvement in the thermal stability of the PHBV-rich phase, exhibiting a maximum degradation temperature of 313.0 °C, suggests a strong stabilizing effect induced by the compatibilization strategy. These improvements are attributed to the *in situ* formation of branched, higher-molecular weight BioPBS-PBAT-PHBV copolymers during reactive extrusion, which effectively restrict chain mobility and delay thermal degradation.[25] In contrast, the stabilizing effect is less pronounced at a compatibilizer content of 5 wt% (Table 6). This reduction may be associated with grafting-related side reactions commonly observed in degradable polymer systems processed with organic peroxides, such as chain scission, which can result in compatibilizer species with reduced molecular weight.[75]

Table 6 Thermogravimetric analysis for the ternary blends and neat polymers

Sample	Temp. at 5% weight degradation $T_{5\%}$ [°C]	Maximum thermal degradation temperature	
		$T_{max,1}$ [°C]	$T_{max,2}$ [°C]
40-20-40	288.9	303.6	406.2
20-20-60	279.7	305.3	411.1
60-20-20	285.4	302.6	406.8
10-30-60	284.3	299.3	406.0
15-25-60	285.1	301.3	407.3
30-20-50	274.5	292.6	410.3
30-20-50-3	295.9	313.0	421.0
30-20-50-5	289.4	308.8	410.9
PHBV	282.3	303.1	—
BioPBS	357.3	—	410.4
PBAT	340.3	—	408.8

3.5. Scanning electron microscopy (SEM) analysis

SEM was employed to examine the phase morphology, dispersion quality, and interfacial interactions within the PHBV, BioPBS, and PBAT blends. The micrographs provide insights into how the composition and use of compatibilizers influence the internal structure of the materials. For unetched samples, imaging was performed at a magnification of 5000× (Fig. 2a–d). To capture the most representative differences in composition, four distinct formulations, denoted as samples 40-20-40, 20-20-60, 30-20-50 and 30-20-50-3, were selected for detailed evaluation (Table 1). Additional SEM images of the unetched samples are available in the SI (Fig. S5).

The morphology of polymer blends is strongly governed by intrinsic parameters, such as viscosity and miscibility, as well as external processing conditions, including composition ratios, shear forces, and temperature.[76] When polymers are blended in the molten state under shear, two competing mechanisms are commonly observed: droplet breakup, which reduces the size of dispersed domains, and coalescence, which promotes domain growth. The resulting morphology is a consequence of the interplay between these processes and directly impacts the physical and mechanical performance of the blend.[1]

As discussed in section 3.2, the calculated $\Delta\delta$ among PHBV, BioPBS, and PBAT were all below 2.0 $MPa^{1/2}$, suggesting good theoretical miscibility. Additionally, as outlined in section 3.1, the positive spreading coefficient ($\lambda_{PBAT/PBS}$) derived from interfacial tension data (Table 3) suggests that PBS displays complete wetting behavior. This implies that PBS can effectively separate the PHBV and PBAT phases, enhancing the overall interfacial stability of the blend.

Nevertheless, SEM images revealed the presence of voids and interfacial debonding between the PBAT phase and the

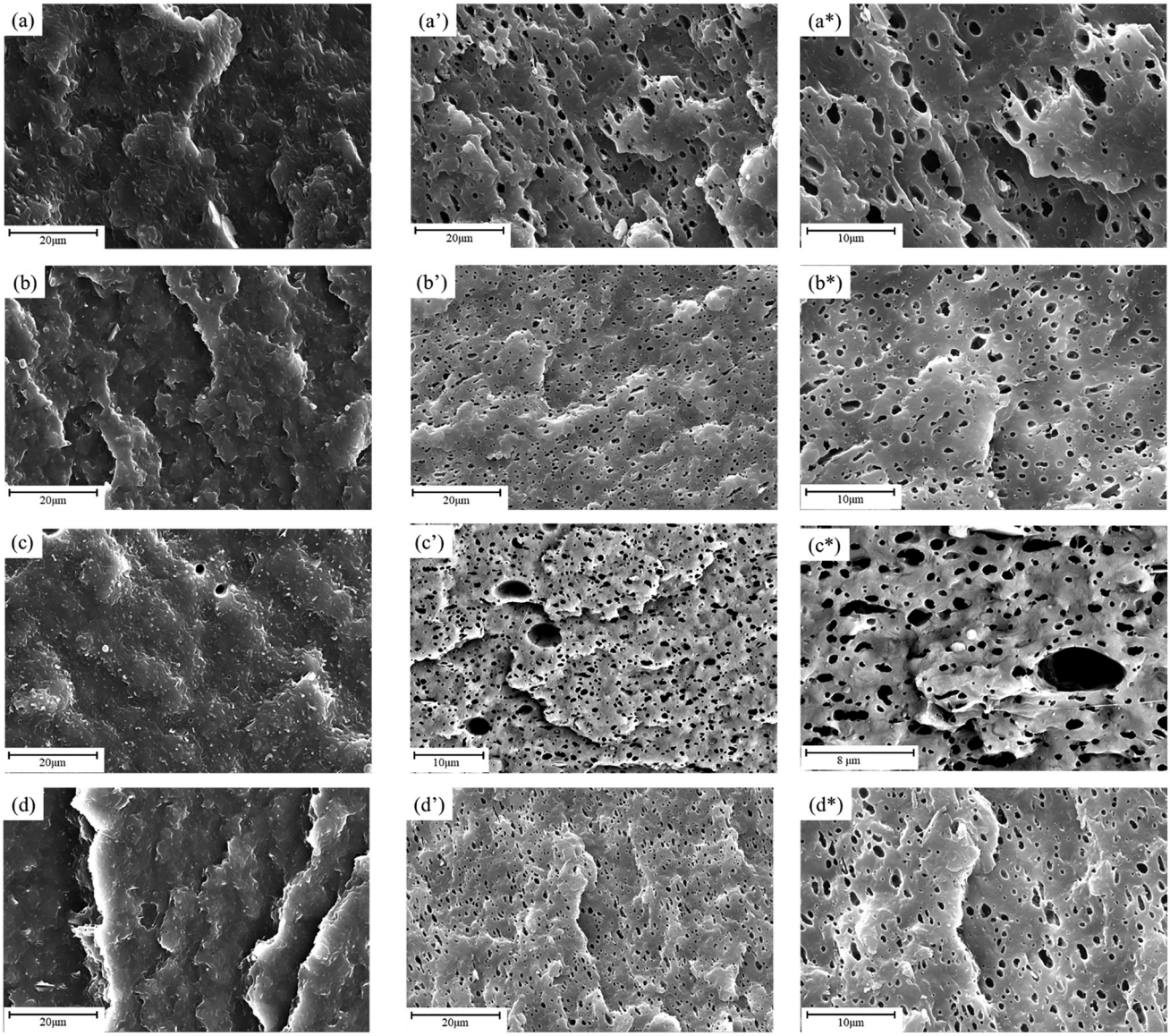

Fig. 2 Scanning electron microscopy images of (a) sample 40-20-40, (b) sample 20-20-60, (c) sample 30-20-50, (d) sample 30-20-50-3. Images marked with a prime indicate the etching sample versions. Images marked with an asterisk indicate the zoomed etching versions. Magnifications used in this work are 5000× and 10 000×. The samples were identified as BioPBS-PBAT-PHBV-compatibilizer.

surrounding matrix, with the extent and nature of these defects depending on whether PHBV or BioPBS constituted the continuous phase. These findings suggest limited interfacial adhesion and poor compatibility among the three polymers, which likely contributes to the modest enhancements in toughness observed in the unmodified blends (see section 3.3). As reported by Mao *et al.*,[77] rough fracture surfaces observed in impact tests are typically indicative of ductile behavior and higher impact resistance, while smooth surfaces are more commonly associated with brittle failure and lower toughness. In this context, a delaminated morphology is more characteristic of brittle materials, whereas a smooth, undistorted surface without voids suggests a tougher structure.[23] Notably, clear voids and cracks were observed in sample 20-20-60, 15-25-60 and 30-20-50 (Fig. 2b, c and Fig. S5b, SI), which also exhibited the lowest impact strength behavior, as discussed in section 3.3.

To gain deeper insight into the phase distribution, SEM analysis was performed on cryo-fractured and selectively etched samples (Fig. 2a′–d′). THF was employed as a selective solvent to remove the PBAT phase, thereby enhancing the contrast between the remaining polymer phases. All examined blends exhibited at least a biphasic morphology, which is characteristic of immiscible systems and indicates limited compatibility among PHBV, BioPBS, and PBAT. Similar phase-separated structures have been reported in PHBV/PBAT binary blends regardless the composition ratio.[74] Since the PBAT content remained constant in the etched samples (Table 1),

the overall morphology observed in the SEM images was comparable across formulations. Nevertheless, the etched voids left by PBAT removal appeared larger in samples 40-20-40 and 30-20-50 compared to those in samples 20-20-60 and 30-20-50-3 (Fig. 2), suggesting differences in PBAT dispersion or domain size. Furthermore, when PHBV serves as the continuous matrix phase, PBAT and BioPBS tend to disperse more uniformly, and exhibit improved interfacial adhesion with the matrix. In contrast, when PHBV acts as a dispersed phase in the ternary blend, the interfacial bonding is less effective, which may influence the overall morphology and mechanical performance of the system. Zolali and Favis[36] reported that when PBAT content exceeds 30 wt%, it tends to localize within the PBS phase and at the PBS/PHBV interface. Conversely, at lower concentrations, PBAT migrates out of the PBS domain and concentrates primarily at the interface. Interestingly, their findings involved different spreading coefficients than those identified in the present study, which may account for the distinct morphological features observed here. Specifically, the results of this work suggest that PBS exhibits complete wetting behavior, effectively separating the PHBV and PBAT phases and reinforcing the distinct phase separation seen in the SEM images. A more in-depth morphological study, such as AFM, should be conducted to confirm the phase distribution identified in this study.

Two separate dispersed phases within the matrix morphology were observed in samples 40-20-40, 20-20-60, and 30-20-50 (Fig. 2a–c), with either PHBV or PBS forming the outer shell and PBAT occupying the core. A similar morphology was reported by Zhang *et al.*,[10] who studied PLA/PBS/PHBV ternary blends. Their results showed that core–shell structures formed depending on the dominant matrix (either PLA or PBS), and that changes in matrix selection significantly influenced the overall morphology and mechanical performance, aiming to balance stiffness and toughness.

To address the limited interfacial adhesion among the polymers, a hybrid compatibilizer was incorporated at concentrations of 3 wt% and 5 wt% into formulation 30-20-50. This adjustment aimed to lower the interfacial tension between the immiscible polymer phases. SEM images of the compatibilized samples, 30-20-50-3 and 30-20-50-5 (Fig. 2d and Fig. S5d, SI), displayed a more homogeneous and smoother surface compared to the unmodified formulation 30-20-50 (Fig. S5c, SI), which showed pronounced voids. These morphological improvements align with the enhanced impact strength reported in mechanical results (section 3.3), further confirming the compatibilizer's effectiveness in improving phase interaction and mechanical properties. Additionally, the selectively etched image of sample 30-20-50-3 revealed smaller PBAT voids, further indicating improved compatibility between the polymer phases. These observations support the notion of better phase dispersion and interfacial contact, which will be further discussed in the rheological analysis presented in section 3.7. Similarly, Pesaranhajiabbas *et al.*[25] investigated the effect of incorporating a compatibilizer into a PHBV/PBAT binary blend. Through SEM analysis of selectively etched samples, they observed a reduction in both PBAT particle size and size distribution. This behavior was attributed to enhanced interfacial chemical interactions, which lowered the interfacial tension and inhibited coalescence of the dispersed phase, ultimately stabilizing the blend morphology.

3.6. Fourier transform infrared spectroscopy (FT-IR)

ATR-FTIR spectroscopy was utilized to identify the key functional groups present in the BioPBS-PBAT-PHBV blends, as well as in the individual neat degradable polymers, to provide a deeper understanding of their chemical composition. Fig. 3 presents the ATR-FTIR spectra for all samples, while the spectra for the individual neat polymers can be found in Fig. S6 (SI).

Strong absorption peaks, related to C–H vibration and ester carbonyl group, are observed by all three neat polymers around 2970–2930 cm^{-1} and 1718–1730 cm^{-1}, characteristic of aliphatic and aromatic polyesters. BioPBS exhibits several distinctive peaks, 1335, 1165, and 1050 cm^{-1}, associated with $-CH_2$ stretching, –C–O–C– and –O–C–C– vibrations, characteristic of aliphatic polyester backbone.[78] PBAT displays additional aromatic absorption bands, aromatic skeletal vibrations around 1450 cm^{-1}, ester C–O stretching and alkyl and aromatic C–C and C–H vibrations in the range of 1250 and 1100 cm^{-1}. An extra peak locate at 725 cm^{-1} is associated with multiple adjacent $-CH_2$ groups.[23,79] PHBV is identified by $-CH_3$ and C–O–C vibrations in the range of 1380–970 cm^{-1},[23,79] in agreement with previous studies.[58,80,81]

The intensity of characteristic peaks in the blend spectra varies depending on the composition of each formulation. For instance, the higher intensity of the BioPBS-associated band at 1335 cm^{-1} in Sample 40-20-40 indicates its higher BioPBS content, whereas this feature is not observed in sample 20-20-60 (Fig. 3a). On the other hand, 20-20-60 displays stronger absorption band at 976 cm^{-1} is consistent with its higher PHBV. The same trend is can easily observed for the other formulations in Fig. 3b.

Compatibilization effects were further evaluated by comparing the unmodified blend (sample 30-20-50) with compatibilized formulations containing 3 wt% and 5 wt% of the multiphase compatibilizer (samples 30-20-50-3 and 30-20-50-5, respectively). Fig. 3c and d show formation of new functional groups or shifts in existing peaks in the 1275–950 cm^{-1} region, suggesting chemical interactions and structural modifications induced by the compatibilizer. The primary functional groups affected include C–O–C, $-CH_3$, –C–OH, O–C–C, and C–C, as identified in Fig. 3d. According to Gonzalez-Lopez *et al.*,[82] the process begins with the formation of a polymer radical, initiated by a free radical, often at a tertiary carbon site. Subsequently, the anhydride groups may react with hydroxyl groups, particularly terminal hydroxyls, leading to the formation of new functional groups and, consequently, chemical functionalization. These newly formed groups have been previously described in the literature. These results are consistent with the SEM images, which show that the incorporation of a compatibilizer reduces PBAT domain size, thereby improving

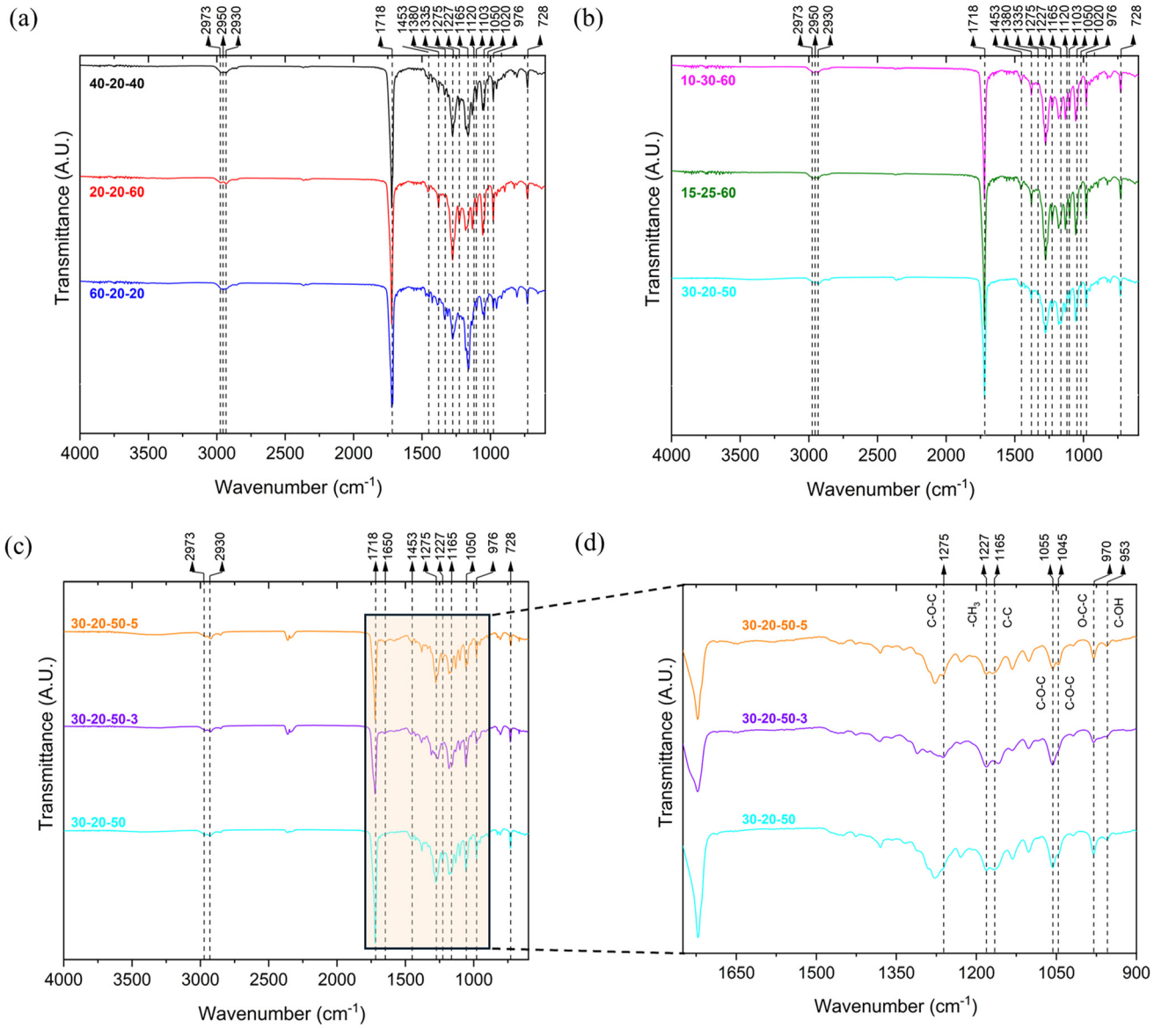

Fig. 3 Transmittance (AU) against wavenumber (cm^{-1}) of (a) sample 40-20-40, 20-20-60, and 60-20-20; (b) sample 10-30-60, 15-25-60, and 30-20-50; (c) sample 30-20-50-5, 30-20-50-3, and 30-20-50, and (d) FTIR spectra highlighted sample 30-20-50-5, 30-20-50-3, and 30-20-50 in the range of 1750 to 900 cm^{-1}. The samples were identified as BioPBS-PBAT-PHBV-compatibilizer.

chemical compatibility between the polymer phases. This enhanced compatibility contributes to improved mechanical properties (section 3.3) and increased polymer entanglement, as indicated by the rheological results (section 3.7).

3.7. Rheological properties

Rheological behavior at processing-relevant temperatures was used to asses macromolecular interactions and structural changes in the blends.[83,84] Fig. 4 illustrates the complex viscosity of neat degradable polymers with their non-compatibilized and compatibilized blend counterparts, while storage modulus, loss modulus, and damping factor (tan δ), are provided in Fig. S7 (SI).

All neat polymers showed a low-frequency Newtonian behaviour flowed by shear-thinning phenomenon at higher frequencies (Fig. 4a). Comparable rheological trends have been widely reported in the literature.[58,74] The blends showed similar trends,, with complex viscosities located between the neat polymer viscosities (Fig. 4a). In particular, samples 40-20-40, 20-20-60, and 60-20-20 exhibited viscosities closer to that of neat PHBV than neat PBAT or BioPBS. This viscosity reduction is likely associated with diminished chain entanglement at the interface between the dispersed and continuous phases.[85] In contrast, blends 10-30-60, 15-25-60, and 30-20-50 exhibited complex viscosities approaching those of neat PBAT and BioPBS, suggesting stronger interfacial interactions and a

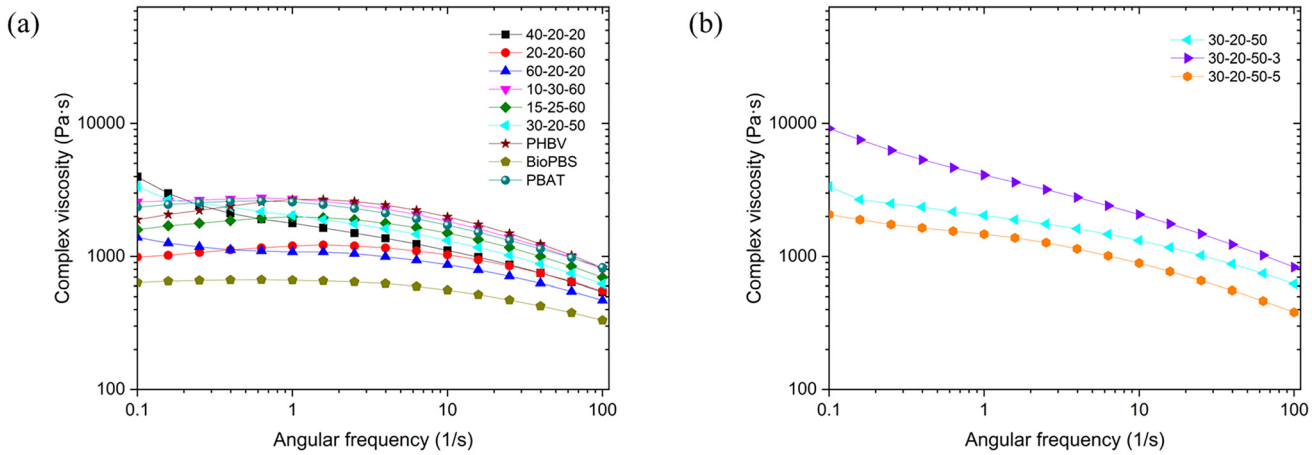

Fig. 4 Rheological properties: (a) complex viscosity of neat polymers and their non-compatibilized and compatibilized blends; (b) comparison of complex viscosity of non-compatibilized blend 30-20-50 with the compatibilized blends 30-20-50-3 and 30-20-50-5. The samples were identified as BioPBS-PBAT-PHBV-compatibilizer.

higher degree of chain entanglement within these un-compatibilized systems.

The effect of the compatibilizer on rheological behavior can be observed in Fig. 4b. Comparing the complex viscosity of blends 30-20-50 and 30-20-50-3, it can be noticed that adding 3 wt% of compatibilizer enhanced the complex viscosity, while adding more compatibilizer in blend 30-20-50-5 reduced this property. The enhanced viscosity of a polymer blend in the presence of compatibilizer has been reported by other researchers in the literature, and it could be attributed to the more interfacial interaction between the blend components in the presence of compatibilizer.[86] Stronger interfacial adhesion increases resistance to flow, thereby raising viscosity, which can be associated with the formation of a more entangled network of BioPBS-PBAT-PHBV copolymers or cross-linked structures induced by reactive species.[87] This trend is in agreement with the enhancement of the mechanical performance (section 3.3) of blend 30-20-50-3 as compared to blend 30-20-50. However, when the content of compatibilizer increased to 5 wt% in blend 30-20-50-5, the viscosity dropped to values even lower than blend 30-20-50. As grafting of polymers in the presence of a peroxide could result in some chain scission, the compatibilizer is supposed to have a lower molecular weight, and consequently lower viscosity.[23] As a result, adding a high level of compatibilizer could contribute to the reduction of blend viscosity. These results also are in concordance with thermal properties (section 3.4).

The tan(δ), which is particularly sensitive to the viscoelastic response of polymer melts, is presented in Fig. S7d (SI). Across the entire frequency range investigated, all neat polymers as well as both compatibilized and un-compatibilized blends exhibit tan(δ) values greater than 1. Among all samples, blends 30-20-50-3 and 30-20-50-5 display tan δ values closest to unity over the full range of angular frequencies, distinguishing them from the other formulations. The comparatively enhanced elastic contribution observed in the compatibilized blends can be attributed to the development of chain entanglements during reactive extrusion. In contrast, a predominantly viscous response suggests insufficient macromolecular entanglement in the molten state.

3.8. Blend cast sheet extrusion

To strengthen this study and demonstrate the applicability of this novel and promising material for flexible packaging applications, cast sheet extrusion was performed using the optimized sample (Fig. S8, SI). Mechanical testing was performed, and the results were summarized in Table 7. The measured properties were generally consistent with those previously reported for injection-moulded specimens (section 3.3). Variations observed between the two sets of results are likely associated with differences in processing methods, since cast-sheet extrusion promotes molecular chain orientation along the machine direction during the stretching stage, leading to a distinct polymer arrangement.[88]

In addition, water and oxygen barrier performances of the extruded cast sheet were evaluated. Their respective OTR, OP, WVTR, and WVP values are summarized in Table 7. The addition of PHBV markedly improved the barrier performance of the blends by reducing both OP and WVP. This behavior is mainly attributed to the high crystallinity of PHBV, which limits molecular diffusion and hinders gas transport through the polymer matrix.[89] These findings were also reported by Pesaranhajiabbas *et al.*,[89] who observed reductions of approximately 50% in OP and 67% in WVP after incorporating 30 wt% PHBV into PBSA. Nevertheless, the permeability values reported for those blends remained considerably higher than those obtained in the present study. The superior barrier performance achieved here is likely associated with the higher PHBV loading (50 wt%), which further enhanced resistance to oxygen and moisture diffusion. Comparable observations were reported by Pal and co-authors,[90] for PBAT/PHBV blends containing 40 wt% PHBV. Their cast-extruded samples exhibited

Table 7 Summary of the mechanical and barrier properties for the cast sheet

30-20-50-3			
Mechanical properties			
σ (MPa)			29.0 ± 1.2
E (MPa)			1189.3 ± 60.7
ε_b (%)			122.4 ± 33.5
Barrier properties			
Oxygen properties		Water vapor properties	
Oxygen transmission rate [cc $(m^2\ day)^{-1}$]	Oxygen permeability [cc mil $(m^2\ day)^{-1}$]	Water vapor transmission rate [gm $(m^2\ day)^{-1}$]	Water vapor permeability [gm mil $(m^2\ day)^{-1}$]
34.2 ± 3.1	260.5 ± 29.1	26.3 ± 1.9	251.0 ± 16.3

OP and WVP values approaching 590 cc mil $(m^2\ day)^{-1}$ and 465 g mil $(m^2\ day)^{-1}$, respectively, which were notably higher than the values measured in the current study.

4. Conclusions

This study tested the hypothesis that the selection of degradable polymers, PBAT, BioPBS, and PHBV, and their relative ratios during extrusion would significantly influence the resulting material properties. A second hypothesis proposed that incorporating a hybrid compatibilizer would enhance interfacial adhesion between polymer phases, thereby improving overall blend performance.

In this work, a novel, fully degradable BioPBS-PBAT-PHBV ternary blend system was successfully developed and systematically characterized. The results confirm both hypotheses: PHBV-rich blends can be formulated without compromising biodegradability while achieving a favorable stiffness–toughness balance. Morphological analysis revealed that the blend components remained largely immiscible across the investigated compositions, despite solubility parameter predictions suggesting miscibility. Interfacial tension measurements further indicated that BioPBS exhibits complete wetting behavior, effectively separating the PHBV and PBAT phases. Importantly, the optimized ternary blend demonstrated synergistic mechanical performance, maintaining a predominantly PHBV-based composition (50 wt%) while achieving close to 100% elongation at break, a tensile strength of 35 MPa, and a Young's modulus exceeding 1.6 GPa. Rheological analysis revealed enhanced interfacial interactions, likely due to increased chain entanglement, even in the absence of a compatibilizer.

The addition of a hybrid compatibilizer at 3 and 5 wt% demonstrated that loading levels significantly influence the final properties, primarily due to competing side reactions such as crosslinking or chain scission. At the lower loading, most properties improved, including elongation at break (8%), impact strength (15%), and Young's modulus (9%). Thermal stability was also enhanced, with the temperature corresponding to 5% weight loss increasing by over 20 °C. These enhancements were attributed to increased chemical interactions at the polymer interfaces, as confirmed by FT-IR, rheological analysis showing higher complex viscosity, and SEM imaging revealing a more homogeneous and smoother surface compared to the unmodified blend.

Overall, these findings demonstrate that combining three degradable polymers can yield materials with tailored mechanical properties suitable for sustainable packaging applications. The incorporation of a hybrid compatibilizer can further enhance performance, though it may induce multiple reactions, including copolymer formation, crosslinking, or chain scission, depending on loading. Future studies will focus on achieving higher miscibility, improved interfacial adhesion, validation of spreading theory, and greater morphological uniformity in these ternary blends. Despite these challenges, the

present study confirms the strong potential of BioPBS/PBAT/PHBV blends as fully biodegradable materials for flexible packaging applications. To demonstrate their industrial applicability, cast sheet extrusion was successfully carried out using the optimized formulation, producing materials with balance mechanical characteristics and high barrier performance. These findings provide a promising pathway toward environmentally sustainable packaging solutions without sacrificing mechanical integrity.

Author contributions

Matias Menossi performed methodologies, investigation, data curation, formal analysis, visualization, and review and editing of the manuscript. Ehsan Pesaranhajiabbas performed methodologies, investigation, data curation, formal analysis, and review and editing of the manuscript. Manushri Gunasekaran performed methodologies, investigation, data curation, formal analysis, visualization, and review and editing of the manuscript. Manjusri Misra performed conceptualization, investigation, methodologies, validation, supervision, resources and funding acquisition, administration, and review and editing of the manuscript. Amar Kumar Mohanty performed conceptualization, investigation, methodologies, validation, supervision, resources acquisition, and review and editing of the manuscript. All authors contributed to discussion, reviews, editing, and approval of the manuscript for publication.

Conflicts of interest

There are no conflicts to declare.

Abbreviations

ΔH_{cryst}	Crystallization enthalpy
ΔH_{melt}	Melt enthalpy
AFM	Atomic force microscopy
ATR	Attenuated total reflectance
BioPBS	Bio-based poly(butylene succinate)
DSC	Differential scanning calorimetry
DHBP	2,5-Dimethyl-2,5-di(*tert*-butylperoxy)hexane
E	Young's modulus
ε_b	Elongation at break
FTIR	Fourier-transform infrared
G'	Storage modulus
G''	Loss modulus
GPPS	General purpose polystyrene
ΔH_m	Melting enthalpy
ΔH_m°	Theoretical melting enthalpy
HDPE	High-density polyethylene
HIPS	High-impact polystyrene
HV	3-Hydroxyvalerate
LDPE	Low-density polyethylene
Lup	Luperox
LDPE	Low-density polyethylene
LLDPE	Linear low-density polyethylene
MA	Maleic anhydride
M_w	Polymer molecular weight
η^*	Complex viscosity
N_2	Nitrogen
OWRK	Owens–Wendt–Rabel–Kaelble
OP	Oxygen permeability
SEBS	Styrene-*b*-(ethylene-*co*-butylene)-*b*-styrene
SEM	Scanning electron microscopy
St	Styrene
δ	Solubility parameters
$\Delta\delta$	Difference of solubility parameters
γ	Surface tension
γ^d	Surface tension, dispersive component
γ^p	Surface tension, polar component
γ_s	Surface tensions at the solid–vapor interface
γ_l	Surface tensions at the liquid–vapor interface
γ_{sl}	Surface tension between the solid–liquid interface
λ_{ij}	Spreading coefficient
σ	Tensile strength
$T_{5\%}$	Degradation temperature at 5% weight loss
tan(δ)	Damping factor
T_c	Crystallization temperature
TD	Transverse direction
T_g	Glass transition temperature
TGA	Thermogravimetric analysis
THF	Tetrahydrofuran
T_m	Melting temperature
T_{max}	Maximum degradation temperature
PA6	Polyamide 6
PBAT	Poly(butylene adipate-*co*-terephthalate)
PBS	Poly(butylene succinate)
PBSA	Poly(butylene succinate-*co*-adipate)
PC	Polycarbonate
PCL	Poly(ε-caprolactone)
PHAs	Polyhydroxyalkanoates
PHB	Polyhydroxybutyrate
PHBV	Poly(3-hydroxybutyrate-*co*-3-hydroxyvalerate)
Phr	Parts per hundred resins
PLA	Poly(lactic acid)
PP	Polypropylene
PPC	Polypropylene carbonate
PS	Polystyrene
W_p	Weight polymer fraction
WVP	Water vapor permeability
X_C	Degree of crystallinity

Data availability

Data for this article, including raw data, origin files for figures and tables are available at [Borealis] at https://doi.org/10.5683/SP3/EZTDLI.

Supplementary information (SI): FTIR comparison between sample 30-20-50 and the hybrid compatibilizer (Fig. S1).

Surface tension components for water and diiodomethane (Table S1). Water and diiodomethane contact angle images for the neat polymers (Table S2). DSC graphs for the ternary blends and neat polymers (Fig. S3). TGA and DTG analysis (Fig. S4), SEM for samples 10-30-60, 15-25-60, 60-20-20, and 30-20-50-5 (Fig. S5). FTIR graph for the neat polymers (Fig. S6). Rheological properties for the ternary blends and neat polymers (Fig. S7). See DOI: https://doi.org/10.1039/d6lp00109b.

Acknowledgements

The authors would like to acknowledge financial support from (i) the Ontario Agri-Food Innovation Alliance – Bioeconomy for Industrial Uses Research Program (Project No. 030648, 030671, 030699 and 030706); (ii) the Natural Sciences and Engineering Research Council of Canada (NSERC), Canada Research Chair (CRC) program Project No. 460788; and the NSERC Discovery Grants Project No. 401716; (iii) NSERC Alliance Grants Program (Project No. 401769) along with the partner industry Competitive Green Technologies, Lamington, Ontario, Canada (Project No. 055427) and the MITACS 2024 Globalink Research Internship Program to carry out this research. This research also benefited from facility funding to the Bioproducts Discovery and Development Centre (BDDC) lab by Fed Dev Ontario, the Ontario Ministry of Agriculture, Food, and Rural Affairs (OMAFRA), the Canada Foundation for Innovation (CFI), and the Federal Post-Secondary Institutions Strategic Investment Fund (SIF) and matching funds from the province of Ontario and numerous University of Guelph alumni.

References

1 M. Menossi, M. Misra and A. K. Mohanty, Biodegradable cellulose ester blends: Studies, compatibilization, biodegradable behavior, and applications. A review, *Prog. Polym. Sci.*, 2025, **160**, 1019.
2 S. Ceballos-Santos, D. B. de Sousa, P. G. García, J. Laso, M. Margallo and R. Aldaco, *Sci. Total Environ.*, 2024, **951**, 175452.
3 J. Liu and L. Zheng, Microplastic migration and transformation pathways and exposure health risks, *Environ. Pollut.*, 2025, **368**, 125700.
4 P. Stoett, V. M. Scrich, C. I. Elliff, M. M. Andrade, N. d. M. Grilli and A. Turra, Global plastic pollution, sustainable development, and plastic justice, *World Dev.*, 2024, **184**, 106756.
5 O. O. Alabi, T. O. Akande, O. J. Gbadeyan and N. Deenadayalu, *RSC Adv.*, 2025, **15**, 40541.
6 M. C. Rillig and A. Lehmann, Microplastic in terrestrial ecosystems Research shifts from ecotoxicology to ecosystem effects and Earth system feedbacks, *Science*, 2020, **368**, 1430–1431.
7 S. RameshKumar, P. Shaiju, K. E. O'Connor and R. Babu, Bio-based and biodegradable polymers - State-of-the-art, challenges and emerging trends, *Curr. Opin. Green Sustainable Chem.*, 2020, **21**, 75–81.
8 J. G. Rosenboom, R. Langer and G. Traverso, Bioplastics for a circular economy, *Nat. Rev. Mater.*, 2022, **7**, 117–137.
9 S. Paquette, M. Menossi, E. Pesaranhajiabbas, H. Khalil, M. Misra and A. K. Mohanty, *Polym. Compos.*, 2025, 4509–4526.
10 K. Zhang, A. K. Mohanty and M. Misra, *ACS Appl. Mater. Interfaces*, 2012, **4**, 3091.
11 Y. Yu and M. Flury, *npj Mater. Sustainability*, 2024, **2**, 1–7.
12 W. Z. Zheng, X. Li, P. Y. Xu, Z. Y. Zhang, P. L. Wang, B. Lu, D. Huang, Z. C. Zhen, J. H. Ji and G. X. Wang, *Resour., Conserv. Recycl.*, 2024, **209**, 107771.
13 S. García-Chumillas, T. Guerrero-Murcia, M. Nicolás-Liza, F. Monzó, A. Simica, L. Simó-Cabrera and R. M. Martínez-Espinosa, *Front. Mater.*, 2024, **11**, 1405483.
14 J. Zhang, V. Hirschberg, M. Pollard, M. Wilhelm and D. Rodrigue, *Resour., Conserv. Recycl.*, 2024, **209**, 107741.
15 M. Ismail, A. Abouhmad, N. Warlin, S. H. Pyo, O. E. Örn, B. Al-Rudainy, C. Tullberg, B. Zhang and R. Hatti-Kaul, *Green Chem.*, 2024, **26**, 3863.
16 N. Nomadolo, A. Mtibe, O. Ofosu, C. Mekoa, J. Letwaba and S. Muniyasamy, *J. Polym. Environ.*, 2024, **32**, 2644.
17 E. M. N. Polman, G. J. M. Gruter, J. R. Parsons and A. Tietema, Comparison of the aerobic biodegradation of biopolymers and the corresponding bioplastics: A review, *Sci. Total Environ.*, 2021, **753**, 141953.
18 S. Lambert and M. Wagner, Environmental performance of bio-based and biodegradable plastics: The road ahead, *Chem. Soc. Rev.*, 2017, **46**, 6855–6871.
19 I. Vroman and L. Tighzert, *Materials*, 2009, **2**, 307.
20 J. Lu, L. Wu and B. G. Li, *ACS Sustainable Chem. Eng.*, 2017, **5**, 6159.
21 A. Rodriguez-Uribe, N. Harder, M. Misra and A. K. Mohanty, *Composites, Part C*, 2023, **12**, 100408.
22 P. Zytner, A. K. Pal, A. K. Mohanty and M. Misra, *Can. J. Chem. Eng.*, 2024, **102**, 2805.
23 M. Menossi, M. Misra and A. K. Mohanty, *ACS Appl. Polym. Mater.*, 2024, **6**, 10202.
24 K. W. Meereboer, M. Misra and A. K. Mohanty, *Green Chem.*, 2020, **22**, 5519.
25 E. Pesaranhajiabbas, A. K. Mohanty and M. Misra, *ACS Appl. Polym. Mater.*, 2025, 2439–2450.
26 S. Chuakhao, J. T. Rodríguez, S. Lapnonkawow, G. Kannan, A. J. Müller and S. Suttiruengwong, *Polym. Test.*, 2024, **132**, 108383.
27 F. Wu, M. Misra and A. K. Mohanty, *Polym. Degrad. Stab.*, 2020, **173**, 109066.
28 V. Mittal, T. Akhtar, G. Luckachan and N. Matsko, *Colloid Polym. Sci.*, 2015, **293**, 573.
29 H. T. Liao and C. S. Wu, *Mater. Sci. Eng., A*, 2009, **515**, 207.
30 M. Menossi, F. Salcedo, N. Rivilli, A. T. Nicolini, V. A. Alvarez and L. N. Ludueña, *J. Polym. Environ.*, 2022, 2114–2137.
31 M. Nofar, R. Salehiyan and M. Barletta, *Polymers*, 2024, **16**, 1699.

32 R. Arrigo, A. D'Anna and A. Frache, *Mater. Today Sustainability*, 2023, 100314.
33 O. Yolacan and S. Deniz, *J. Dispersion Sci. Technol.*, 2025, **46**, 1530.
34 J. Ren, H. Fu, T. Ren and W. Yuan, *Carbohydr. Polym.*, 2009, **77**, 576.
35 M. M. Hedrick, F. Wu, A. K. Mohanty and M. Misra, *RSC Adv.*, 2020, **10**, 44624.
36 A. M. Zolali and B. D. Favis, *J. Phys. Chem. B*, 2016, **120**, 12708.
37 A. Ajji and L. A. Utracki, *Polym. Eng. Sci.*, 1996, **36**, 1574.
38 C. Koning, M. Van Duin, C. Pagnoulle and R. Jerome, *Prog. Polym. Sci.*, 1998, **23**, 707.
39 D. Nath, E. Pesaranhajiabbas, F. Jahangiri, A. Surendren, A. K. Pal, A. Rodriguez-Uribe, M. Misra and A. K. Mohanty, *ACS Omega*, 2024, **9**, 50175.
40 E. Pesaranhajiabbas, A. K. Mohanty, M. S. Al-Abdul-Wahid and M. Misra, *SPE Polym.*, 2024, 217–227.
41 F. Jahangiri, D. Nath, E. Pesaranhajiabbas, A. Surendren, A. K. Pal, A. Rodriguez-Uribe, M. Misra and A. K. Mohanty, *Can. J. Chem. Eng.*, 2025, **103**, 5357.
42 Z. Miao, L. Li, Y.-h. Xie, D. Feng, F. Wu, D. Xie, Y. Liu and Y. Mei, *Polymer*, 2025, **320**.
43 L. Gardella, M. Calabrese and O. Monticelli, *Colloid Polym. Sci.*, 2014, **292**, 2391.
44 D. C. McNeill, A. K. Pal, A. K. Mohanty and M. Misra, *J. Appl. Polym. Sci.*, 2024, **141**, e55166.
45 D. Wang and X. M. Xie, *Polymer*, 2006, **47**, 7859.
46 H. Li, X. Sui and X. M. Xie, *Polymer*, 2017, **123**, 240.
47 I. García-Castellanos, D. Nath, R. Krishnan, M. Misra and A. K. Mohanty, *ACS Sustainable Resour. Manage.*, 2025, **2**, 594.
48 M. Menossi, M. Misra and A. K. Mohanty, *Macromol. Mater. Eng.*, 2025, 2400434.
49 T. Young, *Philos. Trans. R. Soc. London*, 1805, **95**, 65.
50 D. K. Owens and R. C. Wendt, *J. Appl. Polym. Sci.*, 1969, **13**, 1741.
51 A. Falsafi, S. Mangipudi and M. J. Owen, in *Physical Properties of Polymers Handbook*, ed. J. E. Mark, Springer, New York, USA, 2007, pp. 1011.
52 D. J. Greenhalgh, A. C. Williams, P. Timmins and P. York, *J. Pharm. Sci.*, 1999, **88**, 1182.
53 C. M. Hansen, *Prog. Org. Coat.*, 2004, **51**, 77.
54 D. W. Van Krevelen, in *Properties of Polymers*, Elsevier, New York, USA, 1990, pp. 189.
55 K. G. Patel, R. K. Maynard, L. S. Ferguson, M. L. Broich, J. C. Bledsoe, C. C. Wood, G. H. Crane, J. A. Bramhall, J. M. Rust, A. Williams-Rhaesa and J. J. Locklin, *ACS Sustainable Chem. Eng.*, 2024, **12**, 2386.
56 K. W. Meereboer, A. K. Pal, M. Misra and A. K. Mohanty, *ACS Omega*, 2020, **5**, 14221.
57 A. Rodriguez-Uribe, T. Wang, A. K. Pal, F. Wu, A. K. Mohanty and M. Misra, Injection moldable hybrid sustainable composites of BioPBS and PHBV reinforced with talc and starch as potential alternatives to single-use plastic packaging, *Composites, Part C*, 2021, **6**, 100201.
58 P. Feijoo, A. K. Mohanty, A. Rodriguez-Uribe, J. Gámez-Pérez, L. Cabedo and M. Misra, *Int. J. Biol. Macromol.*, 2023, **225**, 1291.
59 F. Jahangiri, A. K. Mohanty, A. K. Pal, S. Shankar, A. Rodriguez-Uribe, R. Clemmer, S. Gregori and M. Misra, *Prog. Org. Coat.*, 2024, **189**, 108270.
60 D. Ahmad, I. van den Boogaert, J. Miller, R. Presswell and H. Jouhara, Hydrophilic and hydrophobic materials and their applications., *Energy Sources, Part A*, 2018, **40**, 2686–2725.
61 M. R. Snowdon, A. K. Mohanty and M. Misra, *ACS Omega*, 2017, **2**, 6446.
62 P. H. Camani, A. G. Souza, R. F. S. Barbosa, N. C. Zanini, D. R. Mulinari and D. S. Rosa, *Chemosphere*, 2021, **269**, 128708.
63 W. D. Harkins and A. Feldman, *J. Am. Chem. Soc.*, 1922, **44**, 2665.
64 S. Y. Hobbs, M. E. J. Dekkers and V. H. Watkins, *Polymer*, 1988, **29**, 1598.
65 L. P. Li, B. Yin, Y. Zhou, L. Gong, M. B. Yang, B. H. Xie and C. Chen, *Polymer*, 2012, **53**, 3043.
66 S. Shokoohi and A. Arefazar, A review on ternary immiscible polymer blends: Morphology and effective parameters, *Polym. Adv. Technol.*, 2009, **20**, 433–447.
67 T. Abate, C. Amabile, S. Chianese, D. Musmarra and R. Muñoz, *J. Mol. Liq.*, 2024, **393**, 123640.
68 A. Forster, J. Hempenstall, I. Tucker and T. Rades, *Int. J. Pharm.*, 2001, **226**, 147.
69 A. M. Mayes, *Macromolecules*, 1994, **27**, 3114.
70 T. Dollase, M. Wilhelm, H. W. Spiess, Y. Yagen, R. Yerushalmi-Rozen and M. Gottlieb, *Interface Sci.*, 2003, **11**, 199.
71 C. B. Roth, K. L. McNerny, W. F. Jager and J. M. Torkelson, *Macromolecules*, 2007, **40**, 2568.
72 B. J. Factor, T. P. Russell and M. F. Toney, *Phys. Rev. Lett.*, 1991, **66**, 1181.
73 G. Dorez, A. Taguet, L. Ferry and J. M. Lopez-Cuesta, *Polym. Degrad. Stab.*, 2013, **98**, 87.
74 P. Zytner, A. K. Pal, F. Wu, A. Rodriguez-Uribe, A. K. Mohanty and M. Misra, *ACS Omega*, 2022, 1946–1956.
75 M. Przybysz, Ł. Zedler, M. R. Saeb and K. Formela, *React. Funct. Polym.*, 2018, **127**, 113.
76 E. Pesaranhajiabbas, A. K. Pal, A. Rodriguez-Uribe, A. K. Mohanty and M. Misra, *ACS Appl. Polym. Mater.*, 2022, **4**, 5546.
77 Z. Mao, X. Zhang, G. Jiang and J. Zhang, *Polym. Test.*, 2019, **73**, 21.
78 A. R. de Matos Costa, A. Crocitti, L. H. de Carvalho, S. C. Carroccio, P. Cerruti and G. Santagata, *Polymers*, 2020, **12**, 2317.
79 D. Meng, J. Xie, G. I. N. Waterhouse, K. Zhang, Q. Zhao, S. Wang, S. Qiu, K. Chen, J. Li, C. Ma, Y. Pan and J. Xu, *J. Appl. Polym. Sci.*, 2020, **137**, 48485.
80 Y. X. Weng, Y. Wang, X. L. Wang and Y. Z. Wang, *Polym. Test.*, 2010, **29**, 579.

81 S. Handali, E. Moghimipour, M. Rezaei, Z. Ramezani and F. A. Dorkoosh, *Pharm. Dev. Technol.*, 2020, **25**, 206.
82 M. E. González-López, J. R. Robledo-Ortíz, R. Manríquez-González, J. A. Silva-Guzmán and A. A. Pérez-Fonseca, Polylactic acid functionalization with maleic anhydride and its use as coupling agent in natural fiber biocomposites: a review, *Compos. Interfaces*, 2018, **25**, 515–538.
83 J. B. Scharnowski, A. Rodriguez-Uribe, A. K. Pal, T. Wang, M. R. Snowdon, M. Misra and A. K. Mohanty, *Macromol. Mater. Eng.*, 2022, **307**, 10202–10217.
84 F. Wu, M. Misra and A. K. Mohanty, *ACS Appl. Polym. Mater.*, 2019, **1**, 1604.
85 Y. Jin, C. Han, Y. Li, H. Cheng, D. Li and H. Wang, *Polymers*, 2023, **15**, 4281.
86 A. Taguet, in *Compatibilization of Polymer Blends: Micro and Nano Scale Phase Morphologies, Interphase Characterization, and Properties*, Elsevier, 2019, pp. 453.
87 F. Wu, M. Misra and A. K. Mohanty, *RSC Adv.*, 2019, **9**, 2836.
88 F. Coffigniez, A. Bessiere and V. Guillard, *J. Food Eng.*, 2026, **406**, 112821.
89 E. Pesaranhajiabbas, A. K. Mohanty, F. M. Defersha and M. Misra, *Composites, Part A*, 2025, 109482.
90 A. K. Pal, F. Wu, M. Misra and A. K. Mohanty, *Composites, Part B*, 2020, **198**, 108141.